

## OPEN ACCESS

## EDITED BY

Ulrich Blank,  
Institut National de la Santé et de la  
Recherche Médicale (INSERM), France

## REVIEWED BY

Julie Gosse,  
University of Maine, United States  
Joakim Dahlin,  
Karolinska Institutet (KI), Sweden

## \*CORRESPONDENCE

Sandro Capellmann  
✉ scapellmann@ukaachen.de  
Michael Huber  
✉ mhuber@ukaachen.de

## SPECIALTY SECTION

This article was submitted to  
Molecular Innate Immunity,  
a section of the journal  
Frontiers in Immunology

RECEIVED 30 January 2023

ACCEPTED 20 March 2023

PUBLISHED 30 March 2023

## CITATION

Capellmann S, Sonntag R, Schüler H,  
Meurer SK, Gan L, Kauffmann M, Horn K,  
Königs-Werner H, Weiskirchen R, Liedtke C  
and Huber M (2023) Transformation of  
primary murine peritoneal mast cells by  
constitutive KIT activation is accompanied  
by loss of *Cdkn2a/Arf* expression.  
*Front. Immunol.* 14:1154416.  
doi: 10.3389/fimmu.2023.1154416

## COPYRIGHT

© 2023 Capellmann, Sonntag, Schüler,  
Meurer, Gan, Kauffmann, Horn, Königs-  
Werner, Weiskirchen, Liedtke and Huber.  
This is an open-access article distributed  
under the terms of the [Creative Commons  
Attribution License \(CC BY\)](https://creativecommons.org/licenses/by/4.0/). The use,  
distribution or reproduction in other  
forums is permitted, provided the original  
author(s) and the copyright owner(s) are  
credited and that the original publication in  
this journal is cited, in accordance with  
accepted academic practice. No use,  
distribution or reproduction is permitted  
which does not comply with these terms.

# Transformation of primary murine peritoneal mast cells by constitutive KIT activation is accompanied by loss of *Cdkn2a/Arf* expression

Sandro Capellmann<sup>1\*</sup>, Roland Sonntag<sup>2</sup>, Herdit Schüler<sup>3</sup>,  
Steffen K. Meurer<sup>4</sup>, Lin Gan<sup>5</sup>, Marlies Kauffmann<sup>1</sup>,  
Katharina Horn<sup>1</sup>, Hiltrud Königs-Werner<sup>6</sup>, Ralf Weiskirchen<sup>4</sup>,  
Christian Liedtke<sup>2</sup> and Michael Huber<sup>1\*</sup>

<sup>1</sup>Institute of Biochemistry and Molecular Immunology, Medical Faculty, Rheinisch-Westfälische Technische Hochschule (RWTH) Aachen University, Aachen, Germany, <sup>2</sup>Department of Internal Medicine III, University Hospital, Rheinisch-Westfälische Technische Hochschule (RWTH) Aachen University, Aachen, Germany, <sup>3</sup>Institute of Human Genetics, Medical Faculty, Rheinisch-Westfälische Technische Hochschule (RWTH) Aachen University, Aachen, Germany, <sup>4</sup>Institute of Molecular Pathobiochemistry, Experimental Gene Therapy and Clinical Chemistry (IFMPEGKC), Medical Faculty, Rheinisch-Westfälische Technische Hochschule (RWTH) Aachen University, Aachen, Germany, <sup>5</sup>Genomics Facility, Interdisciplinary Center for Clinical Research (IZKF), Medical Faculty, Rheinisch-Westfälische Technische Hochschule (RWTH) Aachen University, Aachen, Germany, <sup>6</sup>Electron Microscopy Facility, Institute of Pathology, Medical Faculty, Rheinisch-Westfälische Technische Hochschule (RWTH) Aachen University, Aachen, Germany

Mast cells (MCs) are immune cells of the myeloid lineage distributed in tissues throughout the body. Phenotypically, they are a heterogeneous group characterized by different protease repertoires stored in secretory granules and differential presence of receptors. To adequately address aspects of MC biology either primary MCs isolated from human or mouse tissue or different human MC lines, like HMC-1.1 and -1.2, or rodent MC lines like L138.8A or RBL-2H3 are frequently used. Nevertheless, cellular systems to study MC functions are very limited. We have generated a murine connective tissue-like MC line, termed PMC-306, derived from primary peritoneal MCs (PMCs), which spontaneously transformed. We analyzed PMC-306 cells regarding MC surface receptor expression, effector functions and respective signaling pathways, and found that the cells reacted very similar to primary wildtype (WT) PMCs. In this regard, stimulation with MAS-related G-protein-coupled receptor member B2 (MRGPRB2) ligands induced respective signaling and effector functions. Furthermore, PMC-306 cells revealed significantly accelerated cell cycle progression, which however was still dependent on interleukine 3 (IL-3) and stem cell factor (SCF). Phenotypically, PMC-306 cells adopted an immature connective tissue-like MCs appearance. The observation of cellular transformation was accompanied by the loss of *Cdkn2a* and *Arf* expression, which are both described as critical cell cycle regulators. The loss of *Cdkn2a* and *Arf* expression could be mimicked in primary bone marrow-derived mast cells (BMMCs) by sustained SCF supplementation strongly arguing for an involvement of KIT activation in the regulation of *Cdkn2a/Arf* expression. Hence, this new cell line might be a useful tool to study further aspects of PMC function and to address tumorigenic processes associated with MC leukemia.

## KEYWORDS

KIT, cell cycle, transformation, Mrgprb2, protease, cyclin-dependent kinase inhibitor

## Introduction

Mast cells (MCs) are tissue-resident immune cells of myeloid origin and well-known effectors of type I hypersensitivity (1–3). Besides, MCs can contribute to cancer progression by supporting angiogenesis, extracellular matrix degradation, and epithelial-to-mesenchymal transition (4, 5). The immune response to viral and bacterial infections is fundamentally triggered by MCs as they are strategically located at interfaces between host and environment (3, 6). Therefore, they belong to the first line of defence against intruders and fulfil the task to alert other immune cells to migrate to infected tissues (7, 8). Finally, MCs also contribute to tissue repair and homeostasis in the resolution phase of inflammation by secreting anti-inflammatory IL-10 and helping to remodel the extracellular matrix (9–11).

Understanding fundamental MC functions is often impeded by adequate cellular model systems. One reason is that a prototypical MC does not exist. The term mast cell comprises a heterogeneous cell population that can be classified into multiple subgroups depending on the receptor repertoire, composition of secretory granules and tissue residency (12). Thus, finding *in vitro* models that represent all aspects of different MC subtypes is not possible. Different tissue sources used for isolation and differences concerning *in vitro* differentiation and/or culturing of MCs using various cytokine and growth factor combinations influences analyses of general MC features. Due to the difficulties to isolate mature tissue-derived MCs from human or murine sources, many studies dealing with MCs have been conducted using human MC lines like HMC-1.1, -1.2, LUVA and LAD2 (13–15) or rodent MC lines like RBL-2H3 or L138.8A (16, 17). However, results obtained with these cell lines have to be interpreted with caution. Immortalized leukemic cell lines, like the HMC-1 lines usually contain oncogenic mutations, e.g. in the *KIT* gene (18), which influences studies on MC biology. Furthermore, the HMC-1 cell lines do not express a functional FcεR1 on the cell surface impeding studies on IgE receptor signaling. Likewise, the RBL-2H3 cell line, for instance, shows substantial genomic rearrangements whose consequences are scarcely characterized but certainly affect signaling pathways and cellular physiology in multiple ways (19, 20).

In mouse and rats, MCs are – in a simplified way – divided into two groups based on their histochemical staining properties reflecting different granule mediator content. Connective tissue MCs (CTMCs) typically contain tryptase, chymases, carboxypeptidase A3 (CPA3) and heparin proteoglycans, whereas granules of mucosal MCs (MMCs) lack tryptase and instead of heparin predominantly contain chondroitin sulfate (21). *In vitro*, murine mucosal-like MCs can be obtained from multipotent bone marrow-derived precursor cells, which require a long-lasting differentiation process in the presence of IL-3 and (optionally) stem cell factor (SCF). The resulting MCs are referred to as bone marrow-derived MCs (BMMCs). However, *in vitro* differentiated cultures of murine BMMC frequently result in an incompletely differentiated population of MCs, which morphologically and histochemically do not fully correspond to finally differentiated MCs observed in mouse tissues (22). Connective tissue-like MCs can be isolated from peritoneum – hence they are referred to as murine peritoneum-derived MCs (PMCs) – and subsequently

enriched and expanded in culture in the presence of IL-3 and SCF (23). Challenging about PMCs is, however, that peritoneal lavages often yield only strictly limited amounts of enriched PMCs that cannot be cultured over a longer time period. As a consequence, to extensively characterize PMC biology, plenty of mice need to be sacrificed to yield validated scientific data, which is not in agreement with the 3R principles of animal welfare (24).

To obtain a comprehensive picture of general MC characteristics and functions, a combined approach analyzing cell lines, primary cells and *in vivo* models is required. In the present study, we describe the generation of a PMC-derived spontaneously transformed murine MC line termed PMC-306 that we propose as a new additional tool to study MC biology. We analyzed the MC characteristics in terms of morphology, cell surface marker expression, pro-inflammatory effector responses to different stimuli and protease expression in relation to wildtype (WT) PMCs. We could reveal that the PMC line retained its MC features. PMC-306 cells express functional high-affinity IgE and MRGPRB2 receptors and can therefore be used for respective signaling studies. In addition, we investigated proliferation, survival and the cell cycle pattern of PMC-306, which showed dependence on the cytokines SCF and IL-3. The chromosomal analysis did not reveal major chromosomal abnormalities apart from a heterozygous deletion of regions qC4-qC7 on chromosome 4. This region, amongst others, encodes the cyclin-dependent kinase inhibitor 2A (*Cdkn2a*, also known as INK4A or p16) and *Arf* (also known as p19), both of which function as central cell cycle inhibitors regulating the p53 and Rb pathways (25, 26). Intriguingly, despite the observed heterozygosity of the change on DNA level, mRNA expression of *Cdkn2a* and *Arf* was not detectable in PMC-306 cells. We demonstrated that these aberrations lead to an enhanced cell cycle activity, a strongly increased proliferative capacity and suspect that they might be involved in the mechanism of PMC transformation. We could further induce loss of *Cdkn2a* and *Arf* expression by sustained SCF supplementation of BMMC cultures pointing to a role of constitutive KIT activation in the regulation of *Cdkn2a/Arf* expression. Our initial characterization of PMC-306 provides the basis for using this cell line in prospective studies as a new tool to address differential MC functions.

## Material and methods

### Animals and cell culture

Murine peritoneal MCs (PMCs) and bone marrow-derived MCs (BMMCs) were isolated and cultured as described previously (23). Primary WT PMCs were cultured in conventional cell culture medium [RPMI1640 (Invitrogen, #21875-0991) containing 15% FCS (Capricorn, #FBS-12A), 10 mM HEPES (pH 7.4), 50 units/ml Penicillin and 50 mg/ml Streptomycin, 100 μM β-mercaptoethanol, 30 ng/ml IL-3 from X63-Ag8-653 conditioned medium (27) and approximately, depending on its biological activity, 20 ng/ml SCF from CHO culture supernatant (23)]. For cultivation of PMC-306 cells, the amounts of FCS and SCF were reduced from 15% to 10% and from

20 ng/ml to 5 ng/ml, respectively. Primary BMDCs were cultivated like PMCs, however, SCF was only supplemented to analyze the influence of KIT activation. PMC-306 cells were frozen at  $-150^{\circ}\text{C}$  in 90% FCS and 10% DMSO in aliquots of  $10 \times 10^6$  cells per ml. WT PMCs were freshly isolated and were cultured for a maximum of 8 weeks. All mice used in this study were on a mixed C57BL/6 x 129/Sv background. Experiments were performed in accordance with German legislation governing animal studies and following the principles of laboratory animal care. Mice were held in the Institute of Laboratory Animal Science, Medical Faculty of RWTH Aachen University. The institute holds a license for husbandry and breeding of laboratory animals from the veterinary office of the Städteregion Aachen (administrative district). The institute follows a quality management system, which is certified according to DIN EN ISO 9001:2015. All protocols are reviewed by a Governmental Animal Care and Use Committee at the Landesamt für Umwelt-, Natur- und Verbraucherschutz, Recklinghausen (LANUV). No human samples were used and no experiments were conducted involving living animals. Mice were sacrificed by cervical dislocation to isolate cells either from peritoneum to enrich PMCs or from femurs to obtain bone marrow-derived cells, which were differentiated to BMDCs.

## $\beta$ -Hexosaminidase assay

Measuring Fc $\epsilon$ R1-dependent degranulation, MCs were preloaded with 0.15  $\mu\text{g/ml}$  IgE (clone Spe-7, Sigma, #A2831) overnight ( $37^{\circ}\text{C}$ , 5%  $\text{CO}_2$ ). This step was skipped when cells were stimulated *via* MRGPRB2. Cells were washed in sterile PBS, resuspended at a density of  $1.2 \times 10^6$  (PMC-306 line) or  $0.6 \times 10^6$  (WT PMCs) per ml in Tyrode's buffer (130 mM NaCl, 5 mM KCl, 1.4 mM  $\text{CaCl}_2$ , 1 mM  $\text{MgCl}_2$ , 5.6 mM glucose, and 0.1% BSA in 10 mM HEPES, pH 7.4) and allowed to adapt to  $37^{\circ}\text{C}$  15 min. For stimulation, different concentrations of antigen (Ag; DNP-HSA, Sigma, #A6661), Mastoparan (Sigma, #M5280) or Compound 48/80 (C48/80) (Sigma, #C2313) were applied for 30 minutes. The amount of released  $\beta$ -hexosaminidase was determined by an enzymatic assay as described in (28). Degranulation was calculated as

$$\% \text{ Degranulation} = \frac{\text{amount of released } \beta\text{-hexosaminidase}}{(\text{amount of released } \beta\text{-hexosaminidase} + \text{amount of intracellular } \beta\text{-hexosaminidase})}$$

## Cytokine ELISA

To determine IL-6 and TNF secretion, WT PMCs and PMC-306 were stimulated as indicated in the respective experiments. If cells were stimulated with Ag, MCs were pre-loaded with IgE. Cell number was adjusted to  $1.2 \times 10^6/\text{ml}$  in stimulation medium [RPMI 1640 + 0.1% BSA (Serva, #11930.04)], cells were allowed to adapt to  $37^{\circ}\text{C}$  and stimulated for 3 hours. Supernatants were collected after centrifugation. 96-well ELISA plates (Corning, #9018) were coated with capturing anti-IL-6 (1:250, BD Biosciences, #554400) or anti-TNF (1:200, R&D Systems, #AF410-NA) antibodies diluted in PBS

overnight at  $4^{\circ}\text{C}$ . ELISA plates were washed three times with PBS + 0.1% Tween and subsequently blocked with PBS + 2% BSA (IL-6 ELISA) or PBS + 1% BSA + 5% sucrose (TNF ELISA) for 90 min before loading the supernatants (50  $\mu\text{l}$  for IL-6 ELISA, 100  $\mu\text{l}$  for TNF ELISA). Additionally to loading of supernatants, IL-6 (BD Pharmingen, #554582) and TNF (R&D Systems, #410-MT-010) standards in 1:2 dilutions were added and plates were incubated overnight at  $4^{\circ}\text{C}$ . Thereupon, plates were washed three times again followed by incubation with biotinylated anti-IL-6 (1:500, BD Biosciences, #554402) and anti-TNF antibodies (1:250, R&D Systems, #BAF-410) diluted in PBS+1% BSA for 45 minutes and 2 hours, respectively, at room temperature (RT). After 3 washing steps, Streptavidin alkaline phosphatase (SAP, 1:1000, BD Pharmingen, #554065) was added for 30 minutes at RT. After 3 more washing steps, the substrate p-Nitro-phenyl-phosphate (1 pill per 5 ml in sodium carbonate buffer (2 mM  $\text{MgCl}_2$  in 50 mM sodium carbonate, pH 9.8), Sigma, #S0942-200TAB) was added and  $\text{OD}_{450}$  was recorded using a plate reader (BioTek Eon).

## Flow cytometry, viability assay, LAMP-1 assay and cell cycle analysis

Flow cytometry was performed to analyze MC surface marker expression. Roughly  $0.5 \times 10^6$  cells were washed in FACS buffer (PBS + 3% FCS + 0.1% sodium azide) and stained with either FITC-coupled anti-Fc $\epsilon$ R1 (1:100, clone MAR-1, BioLegend, #134306) and PE-coupled anti-CD117 (1:100, clone 2B8, BioLegend, #105808) or FITC-coupled anti-ST2 (1:100, clone DJ8, MD Bioproducts, #101001F) and PE-coupled anti-CD13 (1:100, clone R3-242, BD Pharmingen, #558745), respectively, for 20 minutes at  $4^{\circ}\text{C}$  in the dark. Thereupon, cells were washed again in FACS buffer, resuspended in 200  $\mu\text{l}$  FACS buffer and analyzed using a FACSCanto II (BD Biosciences).

To determine viability of WT PMCs and PMC-306 cells, cells were seeded at a density of  $0.3 \times 10^6$  (PMC-306) or  $0.5 \times 10^6$  (WT PMCs) cells/ml and incubated under different cytokine deprivation conditions for 72 hours. Thereupon, cells were washed in FACS buffer and stained with Annexin V (1:100, BioLegend, #640912) diluted in culture medium for 20 minutes at  $4^{\circ}\text{C}$  in the dark. Immediately before analysis by flow cytometry using the FACSCanto II, propidium iodide (Sigma, #P4864) at a concentration of 1  $\mu\text{g/ml}$  was added.

For LAMP-1 assay, MCs were preloaded with IgE (Spe7) overnight. Cells were washed and cell number was adjusted to  $1 \times 10^6$  cells per ml in RPMI 1640 + 0.1% BSA. Stimulation was performed for indicated time points with Ag (DNP-HSA). The reaction was stopped by centrifugation at  $4^{\circ}\text{C}$  followed by staining of cell surface LAMP-1 (CD107a) using FITC-coupled anti-LAMP-1 antibody (clone 1D4B, BioLegend, #121605) for 20 minutes at  $4^{\circ}\text{C}$  in the dark. Cells were washed in FACS buffer and LAMP-1 cell surface expression was determined by flow cytometry using a FACSCanto II.

For analysis of cell cycle parameters, background values of pooled (from  $n=3$  per PMC cell type), unstained cells were subtracted from values of three independent stained samples.

Cultured cells were pelleted by centrifugation (1400 rpm, 4°C, 10 min), subsequently stained with fluorophore-labelled antibodies against the surface markers CD117-PE-Cy7 (1:100, # 561681, BD Biosciences) and FcεR1-FITC (1:100, #11-5895-81, Invitrogen Thermo Fisher Scientific) in FACS-blocking buffer (mixture of 0.66% human/rabbit/mouse serum, Sigma-Aldrich, and 1% Bovine Serum Albumin, Sigma-Aldrich) for 40 minutes at 4°C. Cell fixation and permeabilization was performed using the eBioscience Foxp3/Transcription Factor Staining Buffer Set (Invitrogen Thermo Fisher Scientific) according to the manufacturer's protocol. Intracellular co-staining of cells was performed using a mix of fluorophore-labelled antibodies against pH2Ax-PerCP-Cy5.5 (1:100, #564718, S139, BD Biosciences) together with pH3-AL647 (1:100, #3458, S10, Cell Signaling Technology) or MKi67-AL700 (1:100, #56-5698-82, Invitrogen Thermo Fisher Scientific) diluted in FACS-blocking buffer (mixture of 0.66% human/rabbit/mouse serum, Sigma-Aldrich, and 1% Bovine Serum Albumin, Sigma-Aldrich in PBS) for 30 minutes at 4°C. The cellular DNA content was determined by DAPI staining (BD Pharmingen, 1:1000 in 1x PBS). Compensation of each fluorochrome was automatically performed using OneComp ebeads (#01-111-42, Invitrogen Thermo Fisher Scientific) according to manufacturer's recommendations. Measurements were performed using a BD LSRFortessa (BD Biosciences).

Acquired flow cytometry data were analyzed with FlowJo software v10 (Tree Star).

## RT-qPCR

Total RNA was isolated from 4 x 10<sup>6</sup> cells using NucleoSpin RNA Plus Kit (Macherey Nagel, #740955.50) according to manufacturer's instructions. 1 µg of RNA was reverse transcribed using random oligonucleotides (Roche, #11034731.001) and Omniscript Reverse Transcription (RT) Kit (Qiagen, #205113) according to manufacturer's instructions. Quantification of transcript expression was performed using Sybr green reaction mix SensiFAST (Bioline, #BIO-86005) and 10 pmol of specific primers. PCR reaction was performed on a Rotorgene Q (Qiagen). Transcript expression was normalized to the housekeeping gene *Hprt* and relative expression was calculated according to the delta-C<sub>T</sub> method (29). Following primers were used: *Hprt*-fwd: GCTGGTGAAGGACCTCC, *Hprt*-rev: CACAGGACTAGAACACCTGC, *Cdkn2a*-fwd: CTTTCGGT CGTACCCCGATT, *Cdkn2a*-rev: AGAAGGTAGTGGGG TCCTCG, *Arf*-fwd: TGGTGAAGTTCGTGCGATCC, *Arf*-rev: TACGTGAACGTTGCCCATCA, *Rbl1*-fwd: AACTGAA CCTGGACGAGGGA, *Rbl1*-rev: GAGCATGCCAGCCAGTGT AT, *Dennd4c*-fwd: GGGAGAGACTCTGTGCGCTA, *Dennd4c*-rev: AACGTCTCCACTGCTGCTAC; *Mllt3*-fwd: ATGGC TAGCTCGTGTGCC, *Mllt3*-rev: GAACACCATCCAGTCGT GGG, *Plaa*-fwd: CAGACAGTCCTAACAGGGGC, *Plaa*-rev: TCCTCCAGTGGCAATCAGTC, *Cpa3*-fwd: AATTGCTCC TGTCCTACTTTGA, *Cpa3*-rev: TCACCTAACTCGGAAATCC ACAGT, *Gzmb*-fwd: ATGGCCCCAATGGGCAAATA, *Gzmb*-rev:

CCGAAAGGAAGCACGTTTGG, *Mcpt2*-fwd: TTCACCAC TAAGAACGGTTCG, *Mcpt2*-rev: CTCCAAGGATGAC ACTGATTTCA, *Mcpt4*-fwd: GTGGGCAGTCCCAGAAAGAA, *Mcpt4*-rev: GCATCTCCGCGTCCATAAGA, *Tpsab1* (*Mcpt7*)-fwd: GCCAATGACACCTACTGGATG, *Tpsab1* (*Mcpt7*)-rev: GAGCT GTACTCTGACCTTGTG, *Cma1*-fwd: ACGGACAGAGGTTT TGAGGA, *Cma1*-rev: GAGCTCCAAGGGTGACAGTG, *Mrgprb2*-fwd: CCTCAGCCTGGAAAACGAAC, *Mrgprb2*-rev: CCATCCCAACCAGGGAAATGA, *Ccnd1*-fwd: TCAAGACGG AGGAGACCTGT, *Ccnd1*-rev: GGAAGCGGTCCAGG TAGTTC.

## Stimulation of MCs, western blotting and antibodies

For Ag-dependent MC stimulation, cells were preloaded with IgE (0.15 µg/ml) overnight. For FcεRI-independent stimulation, cells were not preloaded with IgE. Cells were washed with sterile PBS and concentration was adjusted to 1 x 10<sup>6</sup> cells per ml in RPMI1640 + 0.1% BSA. 1 x 10<sup>6</sup> cells were stimulated as indicated. Stimulation was stopped by snap-freezing in liquid nitrogen and subsequent lysis in phosphorylation solubilization buffer (PSB) (50 mM HEPES, 100 mM sodium fluoride, 10 mM sodium pyrophosphate, 2 mM sodium orthovanadate, 2 mM EDTA, 2 mM sodium molybdate, 0.5% NP-40, 0.5% sodium deoxycholate and 0.03% sodium dodecylsulfate (SDS)) for 30 minutes at 4°C. Cell lysates were centrifuged (10 min, 13,000 x g) and subjected to SDS-PAGE and Western blot analysis as described previously (30). The following antibodies were used for detection of p-PLCγ1 (Y783, Cell Signaling Technology (CST), #2821), PLCγ1 (CST, #2822), p-PKB (S473, CST, #9271), PKB (CST, #9272), p-ERK1/2 (T202/Y204, CST, #4370), ERK2 (Santa Cruz, #sc-1647), ERK1/2 (CST, #4696), p-p38 (T180/Y182, CST, #9216), p38 (Santa Cruz, #sc-81621), p-IκBα (S32, CST, #2859), IκBα (CST, #4812), p-KIT (Y719, CST, #3391), KIT (CST, #3074), GAPDH (Santa Cruz, #166574), HSP 90 (CST, #4877), actin (Santa Cruz, #sc-8432), granzyme B (CST, #4275) and trypsinase (Santa Cruz, #sc-32889). Secondary antibodies coupled to horseradish peroxidase were purchased from Dako Cytomation [goat anti-rabbit HRP (#P0448), rabbit anti-mouse HRP (#P0161)].

## Proliferation and XTT assay

Cells were seeded at a density of 0.3 x 10<sup>6</sup> cells per ml (PMC-306) or 0.5 x 10<sup>6</sup> cells per ml (WT PMCs) in medium containing different amounts of cytokines and growth factors or different amounts of Imatinib (Selleckchem, #S1026) using DMSO (Appllichem, #A3072) as control. After 24 hours of incubation in a humidified atmosphere (37°C, 5% CO<sub>2</sub>), cells were resuspended and 50 µl of cell suspension were diluted in 10 ml PBS. Cell count and viability was determined using Casy cell counter (Innovatis). Cell count was monitored over a period of 72 hours.

Metabolic activity was determined using XTT Cell proliferation kit II (Roche, #11465015001). Cells were seeded at a density of 0.3 x

$10^6$  (PMC-306) or  $0.5 \times 10^6$  (WT PMCs) cell per ml in wells of a 96-well microplate and a final volume of 100  $\mu$ l. Metabolic activity was measured after an incubation time of 72 hours under humidified culture conditions (37°C, 5% CO<sub>2</sub>) by adding 50  $\mu$ l of XTT reagent to each well and measuring spectrophotometrical absorbance of the resulting formazan product at a wavelength of 475 nm and a reference wavelength of 650 nm. For analysis, the measured absorbances at 475 nm and 650 nm were blanked to medium controls and for total absorbance the blanked absorbance at 475 nm was subtracted from blanked absorbance at 650 nm (blanked  $A_{475}$  – blanked  $A_{650}$ ). These calculated values are provided in the Figures.

## Electron microscopy

$5 \times 10^6$  primary WT PMCs or transformed PMC-306 were centrifuged and resuspended in 500  $\mu$ l regular growth medium. For fixation, 3% glutaraldehyde dissolved in PBS was added for four hours. The subsequent steps for sample preparations and image acquisition were conducted by the Department of Electron Microscopy at the Institute of Pathology at the University Hospital Aachen. Briefly, the cells were embedded in 5% low-melting agarose (Sigma, #2070-OP), washed in phosphate buffer, post-fixed in 1% OsO<sub>4</sub> (Roth, #8371.1) in 25 mM sucrose buffer and dehydrated by ascending ethanol series (30, 50, 70, 90 and 100%) for 10 min each. Last step was repeated 3 times. Dehydrated specimens were incubated in propylene oxide (Serva, #33715.01) for 30 min, in a mixture of Epon resin (Serva, #21045.01) and propylene oxide (1:1) for 1h and finally in pure Epon for 1h. Samples were embedded in pure Epon and polymerized at 37°C for 12 hours and at 80°C for 48 hours. Ultrathin sections (70–100 nm) were stained with 0.5% uranyl acetate and 1% lead citrate (both EMS, #22400, #17600) to enhance contrast. Samples were viewed at an acceleration voltage of 60 kV using a Zeiss Leo 906 (Carl Zeiss) transmission electron microscope.

## May-Grünwald-Giemsa staining

$1 \times 10^6$  primary PMCs were centrifuged (1,200 rpm, 5 min, 21°C) and resuspended in 100  $\mu$ l PBS. 50  $\mu$ l of the cell suspension was spotted onto an ethanol cleaned glass slide (microscope slides, 76 x 26 mm, pre-cleaned, R. Langenbrink, Emmendingen, Germany) and distributed equally. The glass slide was thoroughly air dried. For the cell line PMC-306  $1.5 \times 10^6$  cells were centrifuged (800 rpm, 5 min, 21°C) and resuspended in 120  $\mu$ l PBS. 40  $\mu$ l of the cell suspension was spotted onto an ethanol cleaned glass slide and distributed equally. The glass slide was thoroughly air dried. The cells were fixed by dipping 10 times in pre-cooled ice-cold acetone (VWR, #20066.296) in a glass tray. Thereafter, the glass slide was thoroughly air dried. The staining of MCs with the MGG stain was performed automated according to standard procedures. Microscopic analysis was done by using a slide scanner device (“Fritz” slide scanner, PreciPoint, Germany) equipped with a 40 x objective and the software MicroPoint (V.2021-01). Higher resolution was obtained by digital zoom. To view or transfer data, the

software ViewPoint (V1.0.0.9628) and ConvertPoint (V1.0.0.299) were used.

## Cytogenetic analysis

Structural and numerical chromosome alterations were investigated by conventional karyotyping of the PMC-306 cell line using GTG banding at a 400 to 550 band level (31). Standard procedure to obtain metaphase spreads were performed (32). Cell division was blocked at metaphase followed by hypotonic treatment and methanol/acetic acid fixation (3:1). The banding techniques included use of a trypsin pre-treatment, which was done according to standard protocols (33). Microscopic evaluation was performed using Axioplan fluorescence microscope (Carl Zeiss) and IKARUS digital imaging systems (MetaSystems). 18 to 24 GTG banded metaphases were analyzed.

## Next generation sequencing

$5 \times 10^6$  cells were harvested directly from the respective cell cultures of primary WT PMCs and PMC-306 and washed in PBS. Cell pellets were resuspended in RNeasy lysis buffer (Qiagen, #1017980) and stored at -80°C. The quantity of RNA was analyzed with the Quantus Fluorometer (Promega, Madison, USA). RNA quality control was done using the 4200 TapeStation System (Agilent Technologies, Inc., Santa Clara, USA). An RNA Integrity Number (RIN) of at least 7.3 verified the high quality of all included RNA samples. Sequencing libraries were generated from 1000 ng of total RNA using TruSeq Stranded Total RNA Library Preparation Kit (Illumina, San Diego, USA, #20020596). The libraries were run on an Illumina NextSeq500 High Output 150 cycles Kit v2.5 (Illumina, San Diego, USA, #20024906). FASTQ files were generated using bcl2fastq (Illumina) with standard parameters. Samples were then processed using the nf-core/RNA-seq pipeline version 3.5 (34) implemented in Nextflow 21.10.6 (35) using Docker 20.10.12 (36) with the minimal command. In brief, lane-level reads were trimmed using Trim Galore 0.6.7 (37) and aligned to the mouse genome (GRCm39) using STAR 2.7.9a (38). Gene-level and transcript-level quantification was done by Salmon v1.5.2 (39).

## Statistical analysis

All data shown were generated from at least three independent experiments. Statistical analysis and graphing of data was performed using GraphPad Prism 9 (GraphPad Software, San Diego, CA 92108). All statistical test procedures were done as described in the respective figure legends. *P*-values were considered statistically significant according to the GP style in GraphPad Prism (ns:  $p > 0.05$ , \*  $p < 0.05$ , \*\*  $p < 0.01$ , \*\*\*  $p < 0.001$ , \*\*\*\*  $p < 0.0001$ ). The respective number of independent biological replicates per experiment is indicated in the figure legends.

## Results

The murine peritoneal MC line PMC-306 spontaneously developed from murine WT peritoneum-derived MCs. Primary PMCs were isolated and enriched from mice with a mixed C57BL/6;129Sv genetic background as described previously (23). After a culture period of 3 weeks, purity of the parental PMC culture was verified. The homogenous cell population showed  $\geq 90\%$  double positivity for Fc $\epsilon$ RI and KIT/CD117 (Supplementary Figure 1A). While usually after a maximum of 8 weeks in culture, PMC proliferation and viability decreases, PMC-306 cells showed accelerated proliferation with increasing passages. Besides, PMC-306 could easily be cryopreserved for storage and thawed to be re-cultivated again. These observations led us to characterize the phenotype of the PMC-306 cell line.

### PMC-306 cells are smaller and less granulated than primary WT PMCs

One hallmark of MCs are their secretory granules containing, amongst others, biogenic amines and proteases, which can be released upon stimulation in the process of degranulation (40). Electron microscopy analysis revealed drastically reduced granularity of PMC-306 cells compared to primary PMCs, which showed a cytoplasm densely packed with electron dense and seemingly empty granular structures (Figure 1A). Similarly, primary PMCs exhibited an increased cytoplasm-to-nucleus relation and were larger compared to PMC-306 as shown by MGG staining (Figure 1B). In FACS analysis, reduced granularity and smaller size of PMC-306 was confirmed. The population of primary WT PMCs shifted towards higher SSC intensities and showed more heterogeneity compared to PMC-306 (Figure 1C). Primary WT PMCs express the typical MC markers Fc $\epsilon$ RI, KIT, ST2 and CD13 on the cell surface, which we could show by FACS analysis (Figure 1E, left panel). Though differences appeared in morphological characteristics, PMC-306 stained positive for the four typical MC markers, as well, confirming that PMC-306 cells still had MC characteristics (Figures 1D, E, right panel).

### PMC-306 show increased but still cytokine-dependent proliferation

Established human MC leukemia cell lines like HMC-1.1 and HMC-1.2 are known for their high proliferative capacity and cytokine-independent growth due to mutations in the receptor-tyrosine kinase KIT (13, 41). Therefore, we sought to determine the cytokine dependence and proliferative capacity of PMC-306. We first compared the proliferation rate of PMC-306 to primary PMCs over 3 days in SCF- and IL-3-containing culture medium. PMC-306 had a doubling time of about 24 hours while primary PMCs proliferated marginally within an investigated time frame of 72 h (Figure 2A). Due to the slow proliferation of primary PMCs, we analyzed the impact of IL-3 and SCF withdrawal on the

proliferation only for PMC-306 cells. Both cytokines were reduced independently, while one factor was kept constant. Reduction of IL-3 to 1% and complete withdrawal of IL-3 significantly, but moderately reduced proliferation after 72 hours, while at earlier time points proliferation remained unaffected (Figure 2B). Instead, reducing the amount of SCF had a substantial impact on proliferation of PMC-306. Reduction by 90% substantially attenuated proliferation already at 48 hours after withdrawal. Further reduction of SCF completely abrogated proliferation of PMC-306 (Figure 2C). Additionally, we measured the viability of primary WT PMCs and PMC-306 after 72 hours of incubation under different deprivation conditions. Reducing the amount of IL-3 had no impact on viability of primary PMCs but significantly attenuated the viability of PMC-306 (Figure 2D; Supplementary Figure 2). Reduction of the SCF concentration significantly reduced viability of primary PMCs. However, 10% remaining SCF reduced viability of PMC-306 without affecting viability of WT PMCs. Under harsher SCF deprivation conditions, viability of PMC-306 cells decreased stronger indicating increased SCF dependence of PMC-306 cells over WT PMCs (Figure 2D; Supplementary Figures 2A, B). Interestingly, when metabolic activity under IL-3-depriving conditions was measured, primary PMCs maintained higher metabolic rates compared to a faster decline in metabolic activity of PMC-306 cells (Figure 2F). SCF withdrawal reduced metabolic activity similarly in both cell types (Figure 2F). In line with increased KIT expression and stronger dependence on SCF for survival, PMC-306 cells were more sensitive to KIT inhibition by Imatinib. 1  $\mu$ M of Imatinib was sufficient to significantly reduce metabolic activity in PMC-306 cells while primary PMCs appeared more resistant showing sustained metabolic activity at the same inhibitor concentration (Figure 2G). Conclusively, the PMC-306 cell line is slightly dependent on IL-3, and even more – compared to primary WT PMCs – on SCF for proliferation and survival.

### Ag-dependent MC effector functions of PMC-306 are comparable to primary WT PMCs

Leukemic MCs proliferate fast, while the reaction to stimulatory signals associated with degranulation and cytokine production is often attenuated due to their immature phenotype or loss of receptor expression (e.g. the Fc $\epsilon$ RI  $\alpha$ - and  $\beta$ -subunits in case of HMC-1.1 and -1.2 cells) (42–44). Therefore, we were interested in determining the capacity of degranulation and pro-inflammatory cytokine production of PMC-306 cells in response to different stimuli. The Fc $\epsilon$ RI is known to respond to increasing concentrations of Ag with a bell-shaped dose response curve (45). The activity of released  $\beta$ -hexosaminidase from cytoplasmic granules can be used as readout for degranulation. Alternatively, to the latter bulk measurement, externalization of the granular transmembrane marker LAMP1 can be measured by FACS analysis to quantify the extent and kinetics of granule fusion with the plasma membrane on a single cell basis. PMC-306 and primary PMCs both showed similar bell-shaped dose-response behaviour with

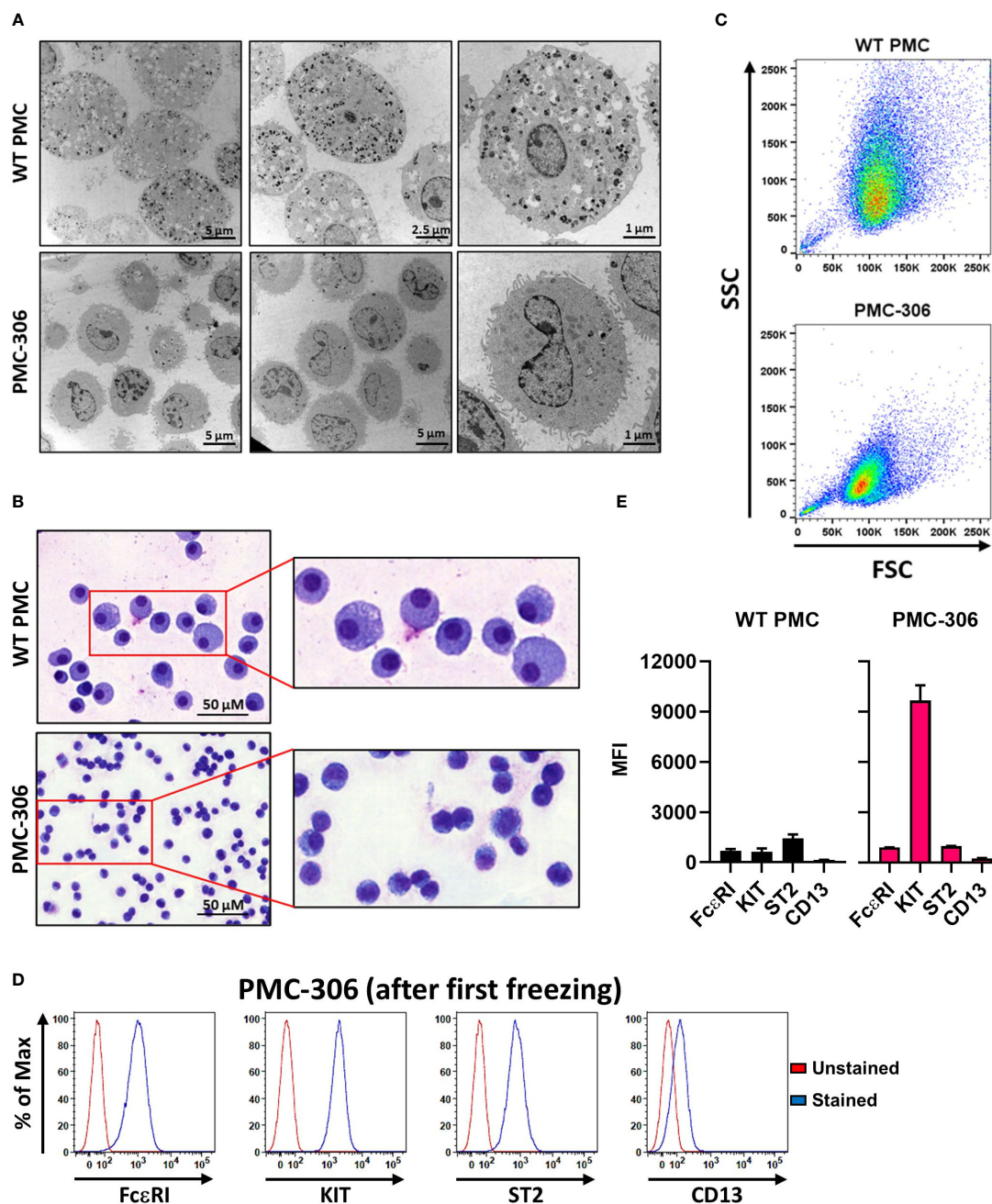


**FIGURE 1**  
 Phenotypic characterization of PMC-306 cells reveals morphological differences to primary WT PMCs. **(A)** Representative electron micrographs of glutaraldehyde-fixed and agarose embedded primary WT PMCs and PMC-306 cells. **(B)** Representative microscopy images of fixed MGG-stained primary WT PMCs and PMC-306 cells. **(C)** Representative FACS analysis of size and granularity of primary WT PMCs in comparison to PMC-306. Forward/side scatter intensities of 30,000 cells were recorded with the same settings to show differences between the two cell types (n=3). **(D)** Representative FACS histograms showing surface localisation of FcεRI, KIT, ST2 and CD13 in PMC-306 cells after freeze-thaw in relation to an unstained control. (n=3) **(E)** FACS analysis of the MC surface markers FcεRI, KIT (CD117), ST2 and CD13. Geometric mean fluorescence intensities (MFI) are plotted for each surface marker (n=4). Data are shown as mean + SD.

increasing Ag concentrations, reaching a maximum release of β-hexosaminidase at 20 ng/ml (Figure 3A). Additionally, we determined the kinetics of degranulation measured as time-dependent LAMP1 externalization. Again, the kinetics of LAMP1 externalization was qualitatively similar between primary PMCs and PMC-306 cells reaching maximal LAMP1 MFIs after 5 minutes of stimulation (Figure 3B). Another receptor triggering MC

degranulation independent of IgE is the GPCR MRGPRB2, which is exclusively expressed in connective tissue-like MCs and can be stimulated by cationic peptides (46–48). Thus, to prove expression of MRGPRB2 in PMC-306, we stimulated primary PMCs and the PMC-306 line with either C48/80 or Mastoparan – compounds that are known to potently activate MRGPRB2 – and measured β-hexosaminidase release. Primary PMCs and PMC-306 both

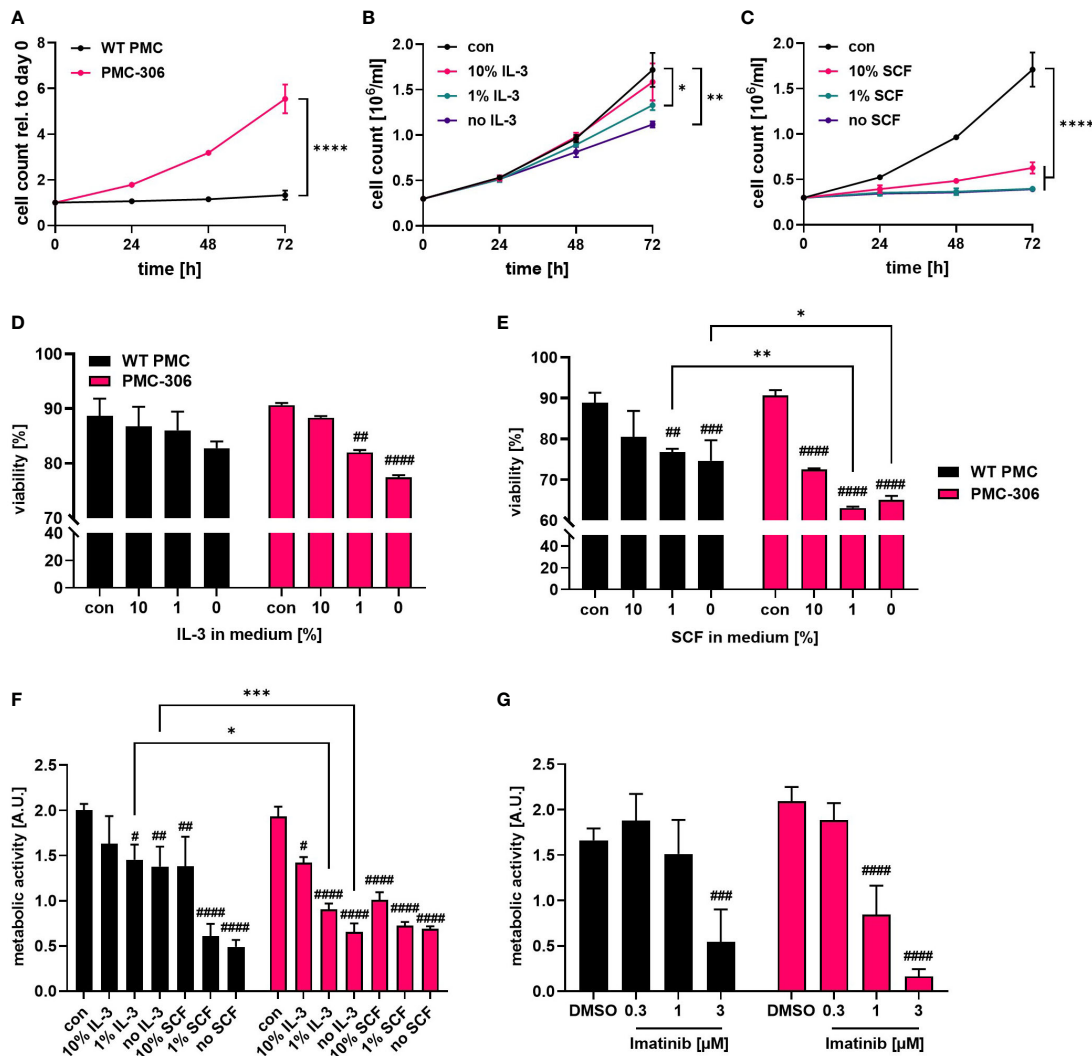


FIGURE 2

PMC-306 show faster proliferation compared to primary PMCs, which is dependent on IL-3 and SCF. (A) Cell number of primary WT PMCs and PMC-306 cells was measured every 24 hours for up to 72 hours using a CASY Cell counter (n=3). Both cell types were cultivated under the same conditions (20 ng/ml SCF and 15% FCS) to allow direct comparison. Proliferation of PMC-306 cells grown under reduced IL-3 (n=3) (B) or SCF (n=3) (C) concentrations was determined every 24 hours up to 72 hours using a CASY Cell counter. Viability of primary PMCs and PMC-306 cells was determined by FACS analysis using Annexin V and propidium iodide staining after 72 hours incubation in medium containing reduced IL-3 (n=3) (D) or SCF (n=3) (E). (F) The metabolic activity of primary PMCs and PMC-306 after 72 hours cultivation under IL-3 or SCF deprivation was determined by XTT assays (n=3). (G) The metabolic activity of Imatinib-treated primary PMCs and PMC-306 cells was determined after 72 hours by XTT assays (n=3). Both cell types, primary PMCs and PMC-306 cells were cultivated under the same medium conditions with the control condition reflecting normal PMC medium containing 20 ng/ml SCF and 15% FCS so that % reduction in SCF refers to the same initial control concentration. Data are shown as mean + SD. (A) Two-tailed, unpaired Student's T test of data at 72 hours. (B, C) One-way ANOVA followed by Tukey multiple comparisons test of data at 72 hours. (D-G) Ordinary two-way ANOVA followed by Sidák multiple comparisons test. *p*>0.05 ns, # and \**p*<0.05, ## and \*\**p*<0.01, ### and \*\*\**p*<0.001, #### and \*\*\*\**p*<0.0001. \* indicates significant differences between groups, while # indicates significant differences relative to control conditions within one group.

degranulated in response to both stimuli in a dose-dependent manner confirming the connective tissue nature of PMC-306 (Figures 3C, D). While degranulation of MCs happens within minutes, secretion of pro-inflammatory cytokines takes several hours of stimulation. We determined secretion of IL-6 and TNF from primary PMCs and PMC-306 in response to FcεRI stimulation. As described above, the response to Ag stimulation followed a bell-shaped dose-response curve in both cell types (Figure 3E). Primary WT PMCs and PMC-306 secreted highest amounts of IL-6 and TNF upon stimulation with 2 and 20 ng/ml Ag

and the pro-inflammatory cytokine response decreased with lower and higher Ag concentrations. This phenocopies the dose response behaviour previously seen for the b-hexosaminidase release in response to increasing Ag concentrations for both cell types. We further observed no pro-inflammatory cytokine secretion in response to TLR4 (LPS), TLR2/6 (FSL-1), KIT (SCF) and MRGPRB2 (C48/80) stimulation at the given stimuli concentrations for both cell types (Figure 3F). Besides, PMC-306 did not react to IL-33 activating the ST2/IL1RAP (IL-1 receptor accessory protein) receptor complex, while primary PMCs secreted

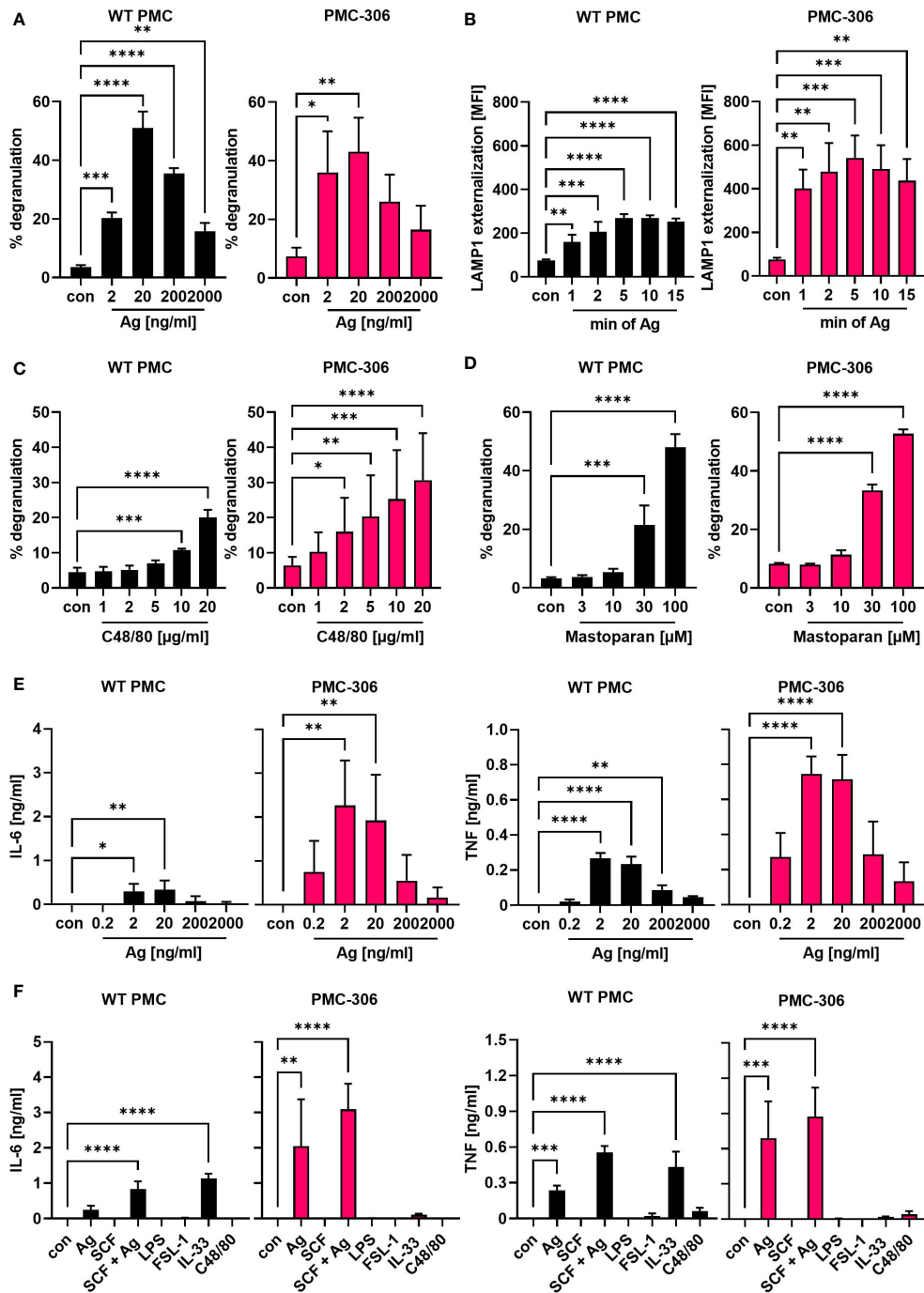


FIGURE 3

The qualitative degranulation and proinflammatory cytokine responses of PMC-306 and primary PMCs are similar. (A) Degranulation of primary WT PMCs (left panel) and PMC-306 cells (right panel) in response to increasing Ag concentrations was determined by  $\beta$ -hexosaminidase release assay (n=3). (B) The time-dependent externalization of LAMP1 was determined by quantifying the LAMP1 on the cell surface in FACS analysis as MFI upon stimulation with 20 ng/ml Ag in primary PMCs (left panel) and PMC-306 cells (right panel) (n=3). The degranulation responses of primary PMCs (left panel) and PMC-306 cells (right panel) to increasing concentrations of the MRGPRB2 agonists C48/80 (C) and Mastoparan (D) were determined by  $\beta$ -hexosaminidase release assays (n=3). The secretion of IL-6 ((E) left) and TNF ((E) right) in response to indicated Ag concentrations was determined by ELISA (n=3). The pro-inflammatory cytokine production of primary WT PMCs and PMC-306 to Ag (20 ng/ml) in comparison to other stimuli (SCF: 100 ng/ml, SCF+Ag: 100 ng/ml and 20 ng/ml, LPS: 1  $\mu$ g/ml, FSL-1: 1  $\mu$ g/ml, IL-33: 10 ng/ml, C48/80: 10  $\mu$ g/ml) was determined by IL-6 ((F) left) and TNF ((F) right) ELISAs (n=3). Data are shown as mean  $\pm$ SD. One-way ANOVA followed by Dunnett multiple comparisons test. Stars indicate significance within one group relative to control.  $p > 0.05$  ns,  $*p < 0.05$ ,  $**p < 0.01$ ,  $***p < 0.001$ ,  $****p < 0.0001$ .

pro-inflammatory cytokines upon IL-33 stimulation. (Figure 3F). Briefly, we could show that the PMC-306 line expresses a functional FcεRI and MRGPRB2 receptor, maintained the ability to degranulate in response to Ag and MRGPRB2 activation but could neither be activated by TLR ligands nor by IL-33 stimulation.

## Signaling pathway activation downstream of typical MC receptors is functional in PMC-306 cells

In comparison to BMMCs, PMCs have a greater active protease repertoire stored within the cytoplasmic granules. This complicates signaling studies and makes protein interaction studies using immunoprecipitation nearly impossible as the lysis of cells in classical lysis buffers containing a mixture of protease inhibitors is not sufficient to prevent protease-dependent protein degradation (12, 40, 49). We therefore aimed to test whether the PMC-306 is suitable for signaling studies upon lysis in normal lysis buffer containing typical protease inhibitors. Further, we wanted to confirm that differential activation of the PMC-306 line leads to comparable activation of signaling pathways as in primary PMCs to verify its suitability for MC signaling studies. Stimulation of PMC-306 with Ag rapidly increased phosphorylation of PLCγ1 at tyrosine 783, which is critical for the initiation of the Ca<sup>2+</sup> response and PKC activation. Activation of the mitogen-activated protein kinases (MAPK) ERK1/2 and p38, as well as phosphorylation of protein kinase B (PKB) occurred within one minute of stimulation, while strongest phosphorylation/activation and degradation of NFκB inhibitor α (IκBα) – a readout for NFκB pathway activation – started at 5 minutes after Ag stimulation (Figure 4A). This indicates that pathways necessary for cytokine production, like the MAPK and NFκB pathways, are functional and strongly responsive to Ag stimulation, which is in line with the described cytokine measurements (Figures 3E, F). Although we could not observe cytokine secretion in response to SCF stimulation, activation of KIT (auto-phosphorylation at Y719) could be detected in response to SCF. However, phosphorylation of KIT, PKB, and MAPK were transient and rapidly decreased after one minute of stimulation (Figure 4B) correlating with the lack of detectable cytokine production, which would require a sustained signal strong enough to induce transcriptional changes in gene expression. Likewise, we could see transient activation of the NFκB and ERK pathways in response to IL-33 though the cytokine production was strongly attenuated compared to WT PMCs (Figure 3F). Interestingly, Y719 of KIT was phosphorylated upon IL-33 stimulation, which corroborates previous findings that revealed a role for KIT in contributing to ST2 signaling in MCs (Figure 4C) (50). Additionally, while most cell lines have substantially elevated basal levels of phosphorylated signaling proteins emerging in Western blot analysis, we did not observe obvious activation/phosphorylation of investigated proteins in PMC-306 cells under unstimulated conditions. Surprisingly, we could not detect considerable cytokine production in response to C48/80 at a concentration of 10 μg/ml, which in previous experiments elicited substantial β-hexosaminidase release (Figure 3C) and was also used in preceding studies to

stimulate MRGPRB2 (46). Yet, we noticed a strong induction of cytokine release in response to 3-fold lower C48/80 concentrations (Supplementary Figure 3A). Accordingly, we used 3 μg/ml C48/80 to analyze activation of MRGPRB2 signaling in the PMC-306 cell line. As shown in Figure 4D, a transient activation of the PKB, ERK and NFκB signaling pathways could be detected after five minutes of stimulation. Notably, the concentrations stimulating cytokine production did not or did only hardly induce degranulation. Besides, stimulation with higher concentrations of C48/80 and Mastoparan previously reported to induce degranulation led to a significant reduction in protein concentration in the cell pellet after lysis, which did not occur with Ag (Supplementary Figure 3B), indicating loss of cellular content upon C48/80 stimulation. Moreover, we were not able to measure an externalization of LAMP1 in response to C48/80 at 10 μg/ml neither in PMC-306 cells (data not shown) nor in primary PMCs (Supplementary Figure 3C) pointing to a substantially different mechanism of degranulation compared to Ag, which potentially involves cellular disintegration.

## Reduced protease expression of PMC-306 suggests an immature phenotype

Our data so far demonstrated that the PMC-306 line still has MC-like properties in terms of morphology and cellular reactivity. Nonetheless, we also noted differences in proliferation and the fact that in contrast to primary WT PMCs, PMC-306 cells have become immortal. Hence, we were interested in transcriptomic differences between PMC-306 and primary WT PMCs that we aimed to uncover by next generation sequencing. For validation of NGS data, we first concentrated on variations in MC granular proteins as the electron micrographs revealed differences in number of granules between WT PMCs and PMC-306. We determined the relative β-hexosaminidase content of equal cell numbers of primary PMCs and PMC-306 and found significantly less β-hexosaminidase activity in cell lysates of PMC-306 (Figure 5A). On mRNA level, we found that expression of the proteases *Cpa3*, *Cma1* and *Gzmb* was reduced compared to WT PMCs but still detectable in PMC-306 (Figures 5B–D). However, we could not detect expression of *Mcpt2*, *Mcpt4* and *Tpsab1* in PMC-306 cells (Figures 5E–G). On protein level, we verified expression of granzyme B and tryptase in primary WT PMCs and could confirm a total lack of tryptase expression in PMC-306 cells. Strikingly, despite residual mRNA expression of *Gzmb* in PMC-306, there was hardly any granzyme B protein present (Figure 5H). This pattern of protease expression in PMC-306 is reminiscent of immature MC precursors, that lack expression of proteases up-regulated in late stages of MC differentiation like *Mcpt2* and *Tpsab1* (51, 52). In addition, we wanted to verify expression of the CTMC-specific receptor MRGPRB2, since we could show similar responsivity between PMC-306 and WT PMCs (Figures 3C, D). Though, PMC-306 cells exhibited significantly reduced mRNA expression of *Mrgprb2* (Figure 5I). However, our data suggests that this does not affect the respective degranulation response (compare Figure 3C).

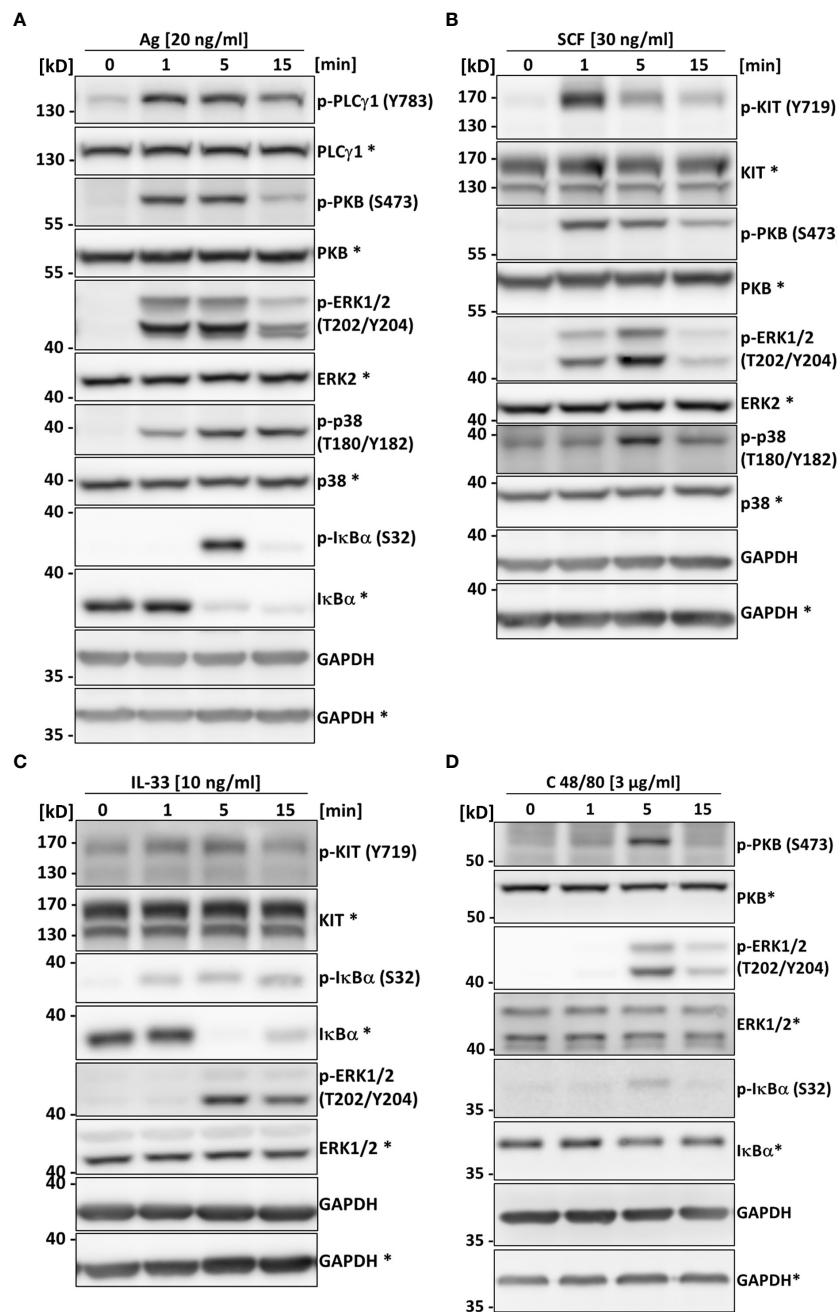


FIGURE 4

The PMC-306 cell line can be used to analyze signaling in response to Ag, SCF, IL-33 and C48/80. The activation of PLCγ1, PKB, the MAPKs ERK and p38, KIT and the NFκB pathway in response to Ag (20 ng/ml) (A) (n=3), SCF (30 ng/ml) (B) (n=3), IL-33 (10 ng/ml) (C) (n=3) or C48/80 (3 µg/ml) (D) (n=3) after 1, 5 and 15 minutes of stimulation was studied by Western blot analysis. Activation of the pathways was analyzed by phospho-specific antibodies (p-PLCγ1 (Y783), p-KIT (Y719), p-PKB (S473), p-ERK1/2 (T202/Y204), p-p38 (T180/Y182), p-IκBα (S32) for key signaling proteins. For loading controls, antibodies recognizing the respective total proteins were used. Asterisks indicate detection on the same membrane. GAPDH served as control for equal loading of both gels. Representative experiments are depicted for each stimulation condition.

As stated in the methods section, we used different culture conditions for primary PMCs and PMC-306 as well as PMC-303 cells. While primary PMCs were cultivated in medium containing 15% FCS and 20 ng/ml SCF, these amounts were both reduced to 10% and 5 ng/ml, respectively, for both cell lines. Our intention was to slow down the enormous proliferation, which – we were afraid – could favour the accumulation of additional mutations rendering the cells genetically more unstable. In initial experiments we

carefully titrated the amounts of SCF and FCS needed to assure proper viability and proliferation of PMC-306 cells avoiding the use of SCF and FCS concentrations that are far beyond the cellular requirements and hence decided for the above-mentioned culture conditions. As we immediately compared mRNA expression of MC proteases between primary PMCs and PMC-306 cells, we aimed at verifying whether this is due to different culture conditions or an actual phenotype of PMC-306 cells. Therefore, we cultivated PMC-

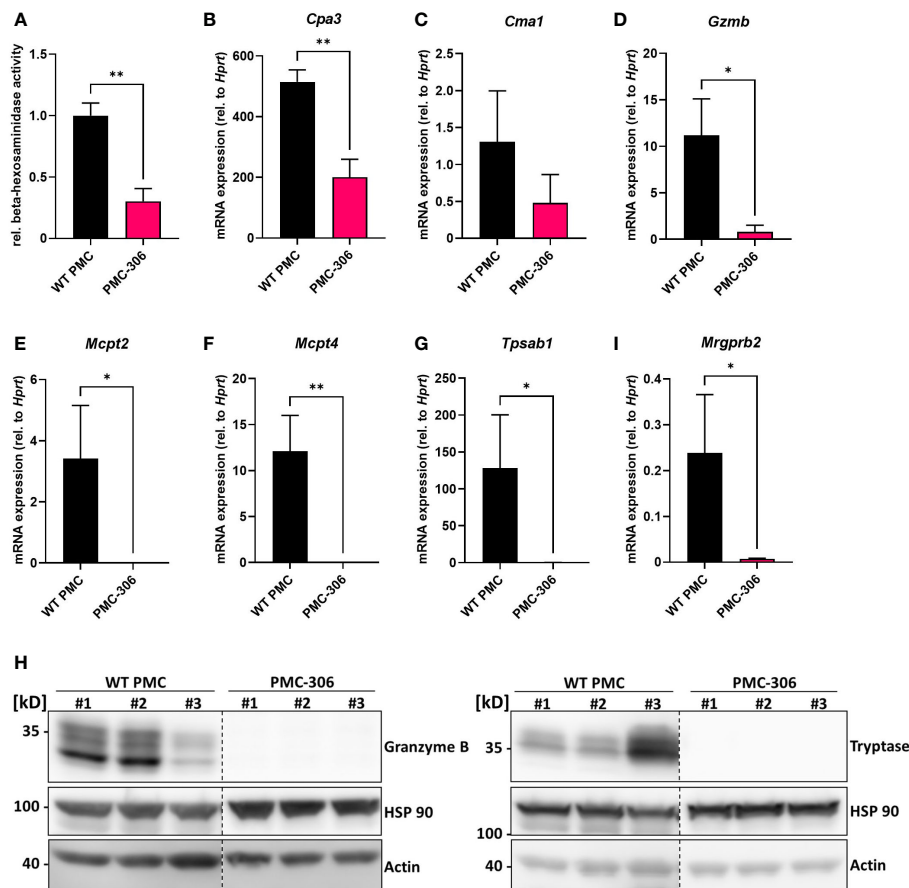


FIGURE 5

The repertoire of protease expression is reduced in PMC-306 cells revealing an immature MC phenotype. (A) The  $\beta$ -hexosaminidase content in primary PMCs and PMC-306 cells was determined by measuring the relative  $\beta$ -hexosaminidase activity in equal numbers of primary PMCs and PMC-306 cells (n=3). (B–G) The protease expression of *Cpa3*, *Cma1*, *Gzmb*, *Mcpt2*, *Mcpt4* and *Tpsab1* (*Mcpt7*) and the expression of *Mrgprb2* (H) were quantified by RT-qPCR in samples from fully differentiated primary PMCs and PMC-306 cells. Data are expressed as mRNA expression relative to *Hprt* determined according to the deltaC<sub>t</sub> method (n=3). (H) Representative Western blots of three lysates from three independent primary WT PMCs and independently taken samples from PMC-306 cells comparing the expression of granzyme B and tryptase on protein level. HSP 90 and actin served as loading controls. Data are shown as mean +SD. Unpaired, two-tailed Student's t-test with Welch's correction. \*p<0.05, \*\*p<0.01.

306 cells in medium containing reduced FCS and SCF as well as in medium containing normal amounts of both FCS and SCF mimicking primary PMC conditions. As depicted in **Supplementary Figures 4A–H**, neither *Cdkn2a/Arf* expression nor expression of *Cma1*, *Cpa3*, *Gzmb*, *Mcpt2*, *Mcpt4* and *Tpsab1* was influenced by higher SCF/FCS concentrations. Besides, mRNA expression of *Mrgprb2* was unaltered irrespective of the medium used for cultivation of PMC-306 cells (**Supplementary Figure 4I**). Moreover, we tested whether the different cultivation conditions changed the size or granularity or affected expression of MC surface markers of PMC-306 cells. Of note, size and granularity as well as the amount of surface-localized Fc $\epsilon$ RI, ST2 and CD13 did not change upon cultivation in medium containing higher amounts of FCS and SCF (**Supplementary Figures 4J, K**). However, KIT expression at the cell surface of PMC-306 cells was significantly reduced under primary PMC-like culture conditions (**Supplementary Figures 4J, K**), which can most likely be attributed to the increased internalization of KIT in response to higher SCF concentrations. In summary, the differences in

cultivation conditions between primary PMCs and PMC-306 cells had only marginal effects on the characterized phenotype of the cell line.

### PMC-306 cells are characterized by a loss of *Cdkn2a* and *Arf* tumour suppressor gene expression

Next, we addressed the question, which genomic or transcriptional alterations are responsible for the transformation and increased proliferation of the PMC-306 line. We first analyzed the karyotype of PMC-306 cells, which revealed a typical male murine diploid (19XY) telocentric set of chromosomes (**Figure 6A**). However, a prominent structural aberration of chromosome 4 characterized by a heterozygous interstitial deletion (Del(4)(C4-C7) was detected (**Figure 6A**, marked by a red arrow). This structural aberration was consistent in all analyzed cells (**Supplementary Figure 4A**) as depicted in **Figure 6B** showing

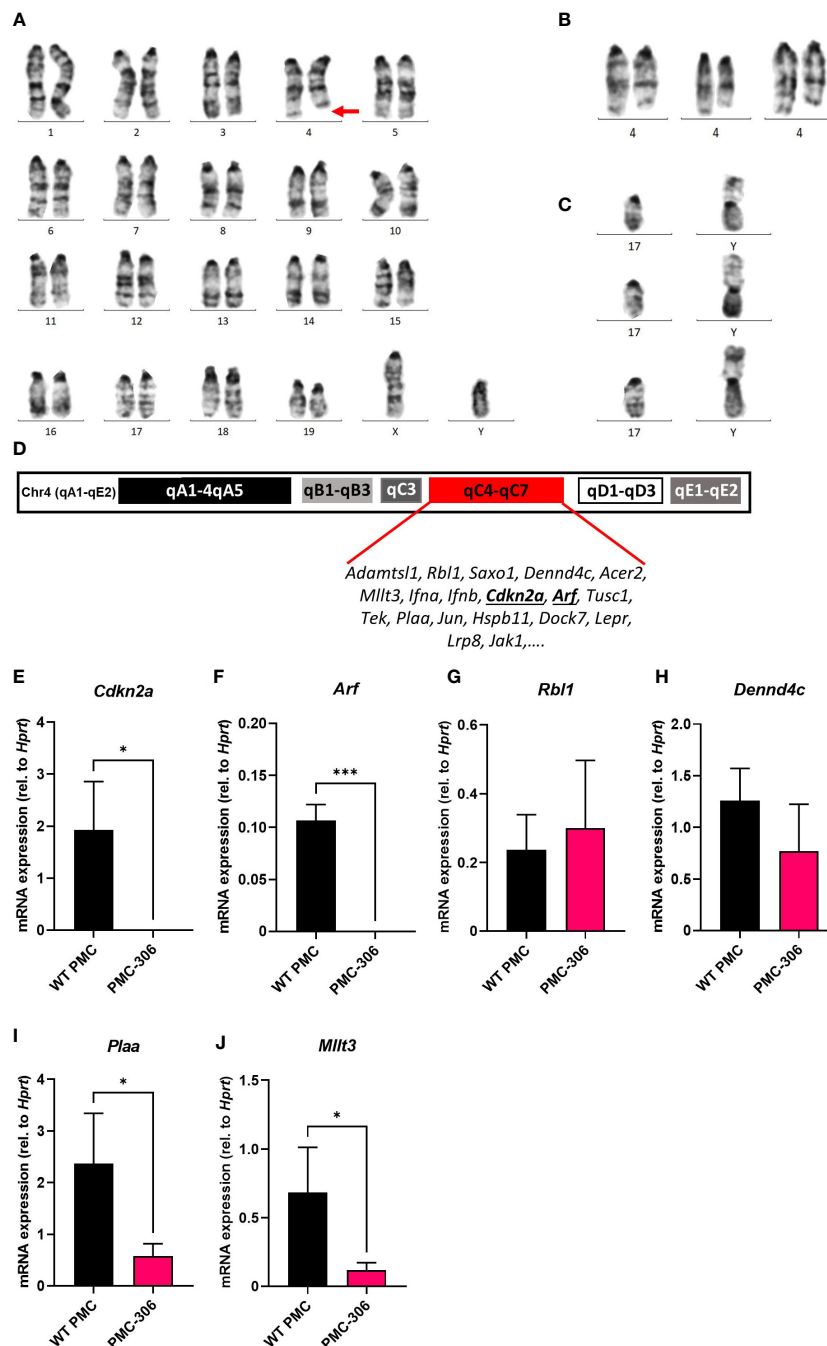


FIGURE 6

Cytogenetic and gene expression analysis identified loss of *Cdkn2a/Arf* expression as potential cause for immortalization of PMC-306. Mitotic chromosomes of PMC-306 were cytogenetically analyzed. (A) Representative image of a conventional G-banded karyotype with structural aberration. Red arrow indicates interstitial deletion of chromosome 4 [Del(4)(C4-C7)]. (B) Further examples of partial karyotypes showing structurally aberrant chromosomes 4 with the same interstitial deletion. (C) Three representative partial karyotypes representing the Y-autosome translocation [T(Y;17)] – confirmed by fluorescence *in situ* hybridization with a Y-specific whole mouse chromosome painting-probe (confirmatory FISH analysis not shown). (D) Architecture of murine chromosome 4 with highlighted region qC4-qC7 and exemplary genes encoded within this region. (E–J) RT-qPCR analysis of *Cdkn2a*, *Arf*, *Rbl1*, *Dennd4c*, *Plaa* and *Mllt3* mRNA expression in primary WT PMCs and PMC-306 cells (n=3). Data are expressed as mean +SD. Unpaired, two-tailed Student’s t test with Welch’s correction. \**p*<0.05, \*\*\**p*<0.001.

three further examples of partial karyotypes of the heterozygously deleted chromosome 4 region (Del(4)(C4-C7). The second most prominent chromosomal aberration represented a Y-autosome translocation [T(Y;17)] (Figure 6C) appearing in roughly one third of analyzed karyotypes (Supplementary Figure 4A), which

has not been described so far so that its significance for the transformation process is presently unclear.

Interestingly, within the heterozygously deleted region of chromosome 4 the INK4/ARF locus is encoded (Figure 6D) (53). p16/INK4A and p19/ARF are responsible for regulation of the RB

and p53 pathways, respectively, thus controlling two essential cell cycle regulators (25, 54). As PMC-306 cells showed a faster proliferation than WT PMCs, we suspected that expression of genes within the INK4/ARF locus might be reduced in PMC-306 cells. We could confirm that mRNA expression of *Cdkn2a* encoding INK4A and *Arf* was not only reduced – as one would expect as a result of a heterozygous deletion – but completely absent in PMC-306 cells (Figures 6E, F). Remarkably, other genes located in the same chromosomal region exhibited a different behaviour. Expression of *Rbl1* and *Dennd4c* was unaffected suggesting that one allele is sufficient to compensate for the deletion of the second (Figures 6G, H), while expression of *Plaa* and *Mllt3* was reduced compared to primary PMCs as one could expect if one allele is lost (Figures 6I, J). Curiously, an independently mutated PMC line, PMC-303, not showing the interstitial deletion on chromosome 4 (Supplementary Figure 4B) also completely lost *Cdkn2a* and *Arf* expression (Supplementary Figures 5C, D), while other genes within the same chromosomal region were not (*Rbl1*, *Mllt3*, *Plaa*) or only slightly (*Dennd4c*) affected (Supplementary Figures 5E–H). In addition, PMC-303 cells showed a trisomy 8 due to a homologous Robertsonian translocation of chromosome 8 (Rb(8.8)) in 24 of 35 analyzed metaphasic spreads (Supplementary Figure 5B), which we did not observe in PMC-306 cells. As we could not identify a prominent chromosomal aberration present in all metaphasic spreads of PMC-303 cells, which might indicate a certain genomic instability, we did not primarily focus on characterizing this cell line. However, we found that similar to PMC-306 cells, also PMC-303 cells remained positive for FcεRI, KIT, ST2 and CD13 in flow cytometry analysis after freeze-thawing the cells (Supplementary Figure 6A). As previously explained for the cultivation of the PMC-306 cell line, we likewise reduced the SCF and FCS concentration in the culture medium of PMC-303 cells, as well. Evaluation of electron microscopy micrographs similarly revealed reduced granularity of PMC-303 cells. This was accompanied by a reduced total β-hexosaminidase content determined by an enzymatic assay measuring β-hexosaminidase activity in cell lysates obtained from equal numbers of primary PMCs and PMC-303 cells (Supplementary Figures 6B, C). Also, in line with what we described for the PMC-306 cell line, PMC-303 cells degranulated in response to C48/80 stimulation suggesting functionality of MRGPRB2 receptor (Supplementary Figure 6D). In addition, PMC-303 cells degranulated to a comparable extent to Ag concentrations between 2 and 200 ng/ml indicating that they are highly sensitive especially to low Ag concentrations and analogously to primary WT PMCs and PMC-306 cells we could measure LAMP1 externalization by flow cytometry upon FcεRI activation starting after 2 minutes after Ag stimulation for up to 15 minutes (Supplementary Figures 6D–F). Finally, the pattern of pro-inflammatory cytokine response of PMC-303 cells towards different stimuli emerged as well similar to PMC-306 cells. While we observed strong IL-6 and TNF production in response to Ag and the co-stimulation of SCF + Ag, there was no detectable cytokine secretion upon triggering of the TLRs TLR4 and TLR2/6 and only a slight but insignificant production of IL-6 and TNF upon IL-33 and C48/80 stimulation (Supplementary Figures 6G, H). Overall, we could establish that PMC-303 cells phenotypically and with respect

to MC characteristics as well as the status of *Cdkn2a/Arf* expression emerged to be highly comparable to PMC-306 cells.

## The PMC-306 cell line has a de-regulated cell cycle

It is well known that uncontrolled proliferation and loss of cell cycle regulation is one of the hallmarks of cancer (25, 54–57). As we have shown above, PMC-306 cells have a strongly accelerated proliferation, which likely is a consequence of the observed loss of *Cdkn2a* and *Arf* expression. Hence, we supposed that in PMC-306 the cell cycle is de-regulated to enable fast proliferation. To prove this, we performed RNAseq with both PMC lines PMC-303 and -306 as well as primary WT PMCs as control. The NGS data have been deposited in NCBI's Gene Expression Omnibus and are accessible through the GEO Series accession number GSE227065 (<https://www.ncbi.nlm.nih.gov/geo/query/acc.cgi?acc=GSE227065>). RNA expression was analyzed from cells directly taken from conventional culture medium without additional treatment. We searched the mRNA expression data for global transcriptomic changes between primary PMCs and the PMC-306 line and focussed on genes that were at least 5-fold regulated. GO enrichment analysis unveiled that the top 15 GO terms were all related to cell cycle, mitosis and cell division (Supplementary Figure 7A). This result led us to investigate the cell cycle by comparing the obtained long-term cultures of spontaneously transformed PMC-306 line with primary WT PMCs using flow cytometry. The gating strategy and unstained controls for background determination for each cell type are shown in Supplementary Figures 7B–D. We first examined cell cycle activity in non-transformed primary WT PMCs and the PMC-306 cell line using the established general cell cycle marker MKI67. As expected, PMC-306 cells revealed substantially (*i.e.* approximately twofold) higher cell cycle activity when compared to primary WT PMCs in terms of MKI67 positive cells (~60–63% vs. 31%) and its expression strength as determined by mean fluorescence intensity (Figures 7A, B). In good agreement, we further detected significantly enhanced mitotic activities in the PMC-306 cells in relation to primary WT PMCs after analyzing phospho-Histone H3 (pH3). PMC-306 cells displayed a higher amount of pH3 positive cells (2%) compared to primary PMCs (1%, Figure 7C). Additionally, we determined the DNA content by DAPI-staining. As expected, MKI67 was found to be expressed in the cell cycle phases Gap1 (G<sub>1</sub>, 2n), DNA-synthesis (S-phase, 2–4n) to Gap2 (G<sub>2</sub>, 4n) and mitosis (M-phase, 4n) in primary WT PMCs and PMC-306 cells (Supplementary Figure 7E, left panel). Furthermore, mitotic active pH3-positive cells were specifically found at a DNA content of 4n in primary PMCs and PMC-306 cells (Supplementary Figure 7E, right panel). Importantly, PMC-306, but not primary PMCs, additionally exhibited an MKI67 and pH3 positive cell fraction with a DNA content above 4n, indicating chromosomal abnormalities such as aneuploidy after the transformation step (Supplementary Figure 7E). Finally, we investigated the DNA integrity by staining of phospho-histone 2Ax (pH2Ax), a well-described marker for DNA-double strand breaks. We found low levels of pH2Ax in WT PMCs (~1%) and slightly

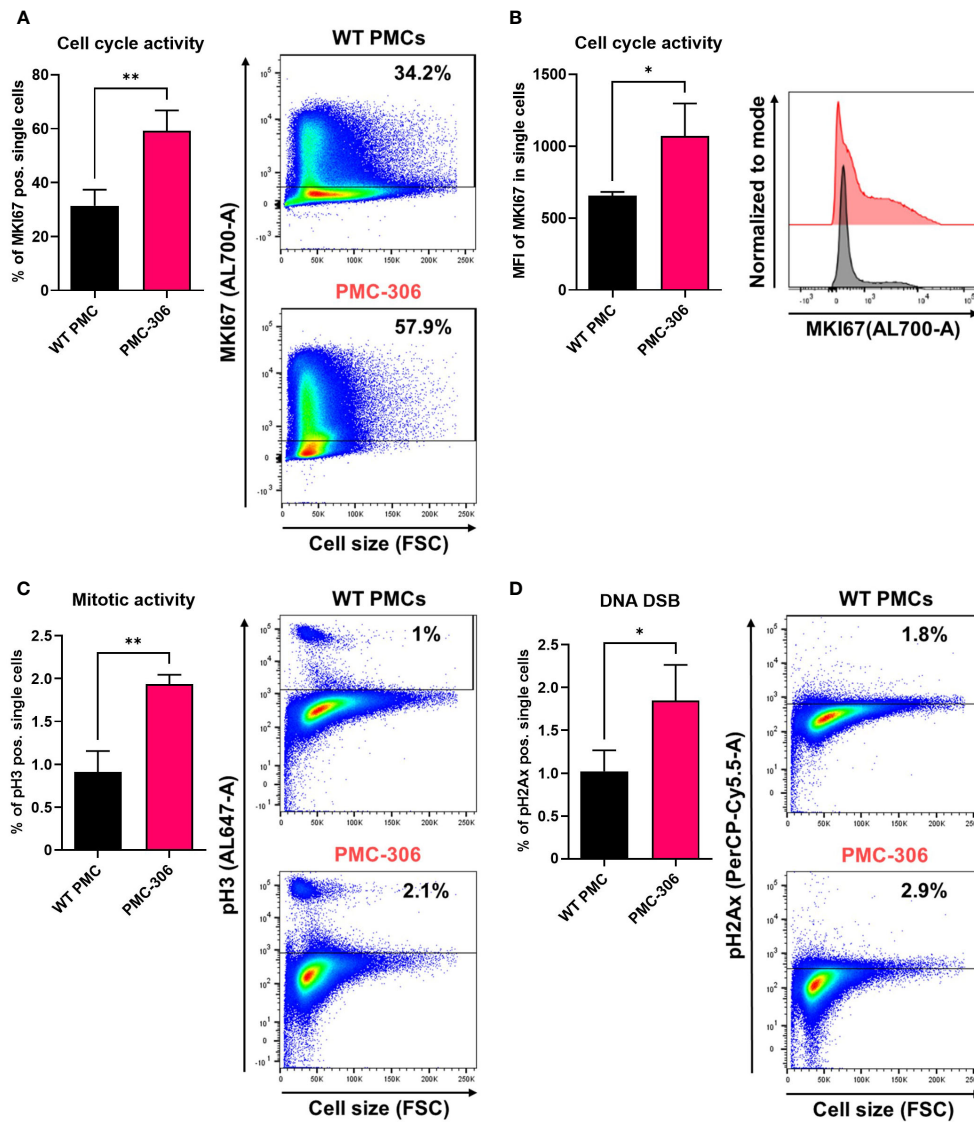


**FIGURE 7**  
 PMC-306 cells are characterized by enhanced cell cycle activity and sporadic DNA damage. The cell cycle of primary WT PMCs was compared to PMC-306 cells. **(A)** Cells were stained with an antibody directed against MKI67 (AL700-A). Left: Quantification of MKI67+ cells (% of single cells, n=3). Right: Representative FACS-plots of MKI67+ cells (% of single cells, n=3). **(B)** Quantification of the mean fluorescence intensity (MFI, n=3) of MKI67 in single cells (left) and a representative histogram showing MKI67 intensities in primary PMCs and PMC-306 cells. **(C)** Cells were stained with an antibody directed against phosphorylated histone H3 (pH3, AL647-A). Left: Quantification of p3+ cells (% of single cells, n=3). Right: Representative FACS-plots of p3+ cells (% of single cells). **(D)** Cells were stained with an antibody directed against phosphorylated Histone H2Ax (pH2Ax, PerCP-Cy5.5-A). Left: Quantification of pH2ax cells (% of single cells, n=3). Right: Representative FACS-plots of pH2Ax+ cells (% of single cells). Data are expressed as mean +SD. Unpaired, two-tailed Student's t test with Welch's correction. \* $p < 0.05$ , \*\* $p < 0.01$ .

increased levels in PMC-306 (~2%, **Figure 7D**). Together, the cell cycle of PMC-306 cells is characterized by a higher mitotic activity, increased DNA damage and aneuploidy.

### Constitutive KIT activation regulates *Cdkn2a* and *Arf* expression in BMMCs

Finally, we aimed at identifying the mechanism for loss of *Cdkn2a/Arf* expression in primary PMCs and suspected KIT activation as a crucial pro-survival and potentially transformation-promoting mechanism due to the occurrence of

frequent KIT mutations in leukemic MC lines (41, 58). Therefore, instead of using PMCs, we analyzed the behaviour of BMMCs, which in contrast to PMCs do not necessarily need SCF for proper differentiation into MCs, and cultivated them from the beginning of the differentiation phase in the absence or presence (mimicking PMC culture conditions) of SCF. We noticed remarkable phenotypic changes of BMMC cultures induced by SCF supplementation. After the differentiation phase of 4 weeks, BMMCs cultivated in the presence of SCF were larger (increased FSC) and more granular (increased SSC) compared to BMMCs from the same mouse only supplemented with IL-3 (**Figure 8A** left two panels, **Figure 8B** left and middle, **Figure 8C** left and middle).

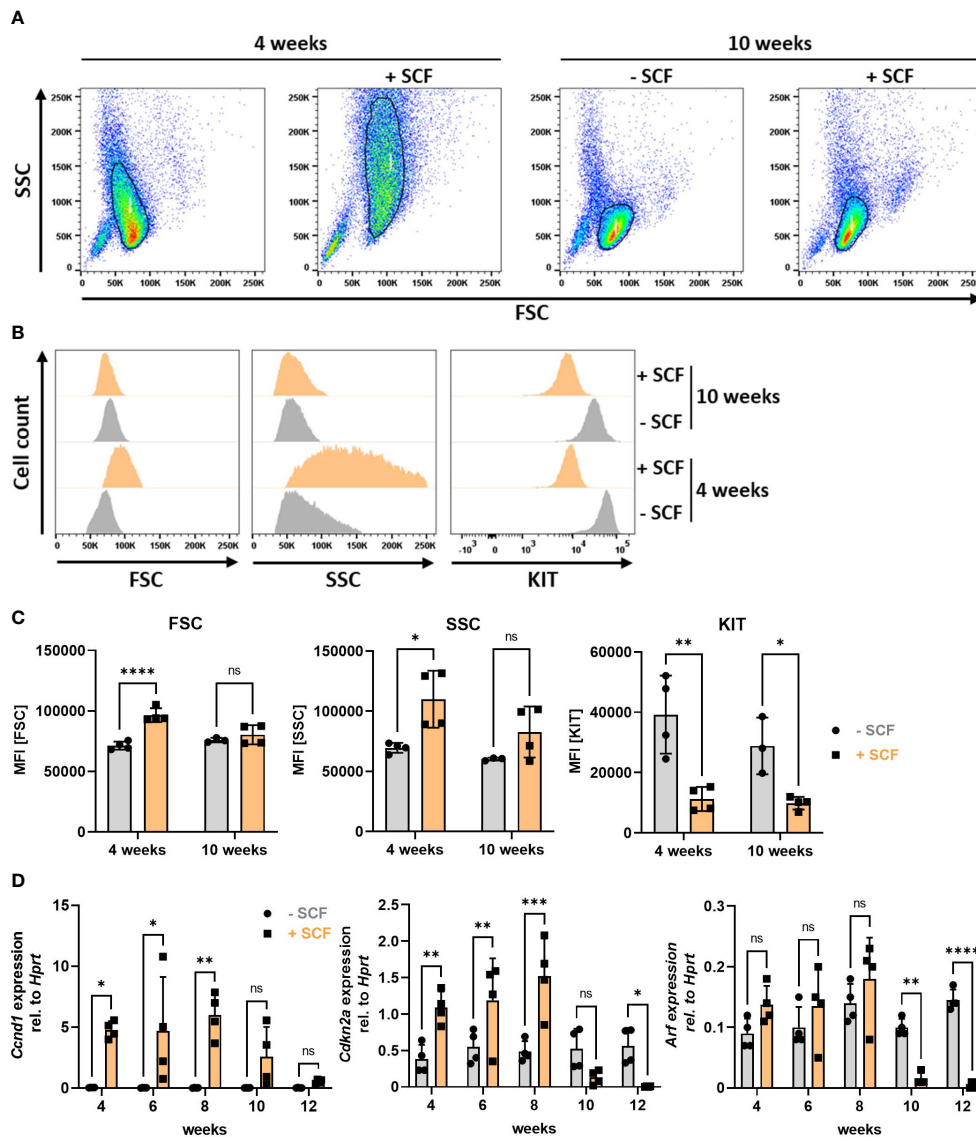


**FIGURE 8**  
 Constitutive KIT activation induces morphological changes and loss of *Cdkn2a/Arf* expression in BMMCs. (A) Representative FACS-plots showing BMMC populations cultivated with or without SCF for 4 (left) or 10 (right) weeks (n=4). (B) Representative histograms showing frequency distributions of forward scatter (left), side scatter (middle) and KIT expression (right) of BMMCs cultivated for 4 or 10 weeks with or without SCF (n=4). (C) Quantified data (MFI) of parameters analyzed in (B) [n=4 for all data except for BMMCs -SCF at 10 weeks (n=3)]. (D) RT-qPCR analysis of *Cnd1*, *Cdkn2a* and *Arf* mRNA expression in BMMCs supplemented or not with SCF over a period of 12 weeks (n=4). Symbols indicate biological replicates. (C) and (D) Ordinary two-way ANOVA followed by Sidák multiple comparisons test.  $p > 0.05$  ns,  $*p < 0.05$ ,  $**p < 0.01$ ,  $***p < 0.001$ ,  $****p < 0.0001$ .

Intriguingly, these morphological differences disappeared after 10 weeks, when size and granularity of SCF-supplemented BMMCs decreased to levels of BMMCs cultivated without SCF (Figure 8A right panels, Figures 8B, C). As a control for SCF treatment we stained for KIT at the cell surface. KIT is known to be internalized upon SCF binding (59). Consequently, less KIT remains on the cellular surface under chronic KIT-stimulating conditions. We could confirm this observation by FACS analysis, as BMMCs supplemented with SCF expressed significantly less KIT at the plasma membrane (Figure 8B right panel, Figure 8C right panel). It is further known that KIT can increase proliferation by inducing transcription of cyclins via the PI3K-AKT pathway (60). Indeed, we

observed increased proliferation of SCF-treated BMMCs and strong upregulation of the G<sub>1</sub>/S cyclin *Cnd1* until 8 weeks. After 10 weeks, however, *Cnd1* expression decreased constantly to levels similar to BMMCs grown in the absence of SCF (Figure 8D, left). Notably, we found a strikingly similar expression pattern for the negative cell cycle regulator *Cdkn2a*, whose expression was increased by SCF supplementation over the first 8 weeks and then dropped to levels below the expression of control BMMCs (Figure 8D, middle). Accordingly, expression of *Arf*, though not significantly increased in the beginning, drastically decreased after 10 weeks in the presence of SCF, as well (Figure 8D, right). Loss of *Cdkn2a* and *Arf* expression thus timely and reproducibly correlates with cell

shrinkage and perfectly mimics the phenotype of PMC-306 cells. Finally, we tested whether BMMCs after 12 weeks of culturing in SCF-containing medium could be cryopreserved. Indeed, we could confirm that specifically SCF-supplemented BMMCs survived freeze-thawing (data not shown). Hence, this observation suggests that constitutive KIT activation might be the driver for cell cycle deregulation and especially prolonged (>10 weeks) SCF supplementation seems to promote decreased *Cdkn2a/Arf* expression

## Discussion

Advancing research of the characteristics and activation mechanisms of MCs either requires the isolation of MCs from donor tissue, *ex vivo* differentiation of human CD34-positive precursor cells or the use of adequate cell lines. Problematically, suitable cell lines with MC-like properties are restricted to few examples with several limitations including loss of FcεRI expression in HMC-1.1, -1.2 and LUVA cells or long doubling times in case of LAD2 cells (14, 15, 42). Thus, MC research is encumbered by MC lines sharing as much features as possible with tissue-resident MCs *in vivo*. Here we present a novel murine MC line, which overcomes these limitations. We showed that the PMC-306 cell line stably expresses a functional FcεRI, has a short doubling time, maintained MC characteristics over multiple passages and is easy to freeze and thaw. These features suggest that PMC-306 cells can be used as a new tool to address questions related to MC research.

We extensively characterized PMC-306 cells and compared their appearance, activation and growth behaviour to non-transformed primary WT PMCs. PMC-306 cells share all characteristics of MCs as they stained positive for the MC surface markers FcεRI, KIT (CD117), CD13 and T1/ST2. We could further demonstrate a strictly IL-3- and SCF-dependent growth and Imatinib sensitivity of PMC-306 excluding KIT activating or Imatinib-resistant mutations, which are often detected in MC leukemia and complicate studies on general MC properties. HMC-1.1 and -1.2 cells bearing KIT mutations have a high basal activity of pro-survival signaling pathways including PI3K/PKB, STAT5 and RAS/RAF/MEK/ERK (58). This complicates studies on signaling pathways activated by other receptors due to enhanced background signals. Importantly, PMC-306 cells, despite cultivated in SCF-containing medium, did not show these high background phospho-signals making them an interesting tool to study MC signaling.

The PMC-306 cell line is derived from primary WT PMCs, which have connective tissue-like MC characteristics. We confirmed this by verifying expression and functionality of the connective tissue MC-specific receptor MRGPRB2. This MC-specific receptor has recently gained attention as its discovery has led to many new insights into the role of MCs in adverse drug reactions, communication with nerve cells and the development of a new tool for skin MC ablation (46, 47, 61). However, studies on the MC activating mechanisms in terms of signal transduction of

MRGPRB2 are scarce. We showed that PMC-306 cells are an appropriate model to study – apart from FcεRI-dependent MC activation – also MRGPRB2-dependent effects. PMC-306 cells substantially reacted to MRGPRB2 activating ligands in terms of degranulation and cytokine production. Strikingly, the results showed that the degranulation seems to involve a completely different mechanism from that of Ag-triggered degranulation as we could not detect externalization of the granular marker LAMP1 and cells significantly lost a bigger part of their protein content within the first minutes of stimulation. A study from Gaudenzio et al. (62) already proposed that MC activation *via* the MRGPRB2 receptor is faster, does not involve compound exocytosis of granules and that the cytokine secretion profile is substantially different in comparison to Ag-dependent degranulation. Nevertheless, they did not deeply look into a mechanistic level how this is regulated by the cell. We further determined the pro-inflammatory cytokine production potential of PMC-306 cells in response to different stimuli. Interestingly, both primary WT and PMC-306 cells potently responded to Ag and IL-33, while TLR agonists like LPS and FSL-1 did not elicit a response. This is in agreement with a proteomic study revealing that primary human connective tissue type MCs lack crucial innate immune receptors including TLR-2, -3, -4, -7, -8 and -11, which is conserved between mouse and human (47). Looking at the overall picture of MC effector functions, there was great similarity between primary WT PMCs and the PMC-306 line.

One hallmark of MCs is their numerous densely packed secretory granules within the cytoplasm storing preformed pro-inflammatory mediators. PMC-306 cells appeared less granulated, showed reduced total β-hexosaminidase content and lacked expression of *Tpsab1*, *Mcpt2*, *Mcpt4* and *Cma1*. However, proteases that appear early in MC differentiation like *Cpa3* and *Gzmb* (52) were still present on mRNA level, which might indicate that the culture of PMC-306 consists of an incompletely differentiated transformed connective tissue MC type. However, GZMB protein expression was entirely absent. This could be a consequence of the drastically increased cell cycle progression, which does not permit the cell to build up complex granular structures resulting in post-transcriptional attenuation of mRNA translation not essential for proliferation. Mechanistically, the lavage of the murine peritoneal cavity may lead to isolation of MCs of different differentiation stages including fully mature and immature MC types. Of note, malignant transformation of myeloid cells often occurs at early differentiation stages, where the proliferative potential is high (52, 63, 64). These circumstances might have contributed to the transformation of the PMC-306 cell line and would well fit to the observed phenotype.

We cultivated primary PMCs and both cell lines, PMC-303 and PMC-306, under different culture conditions. While we strictly followed the established protocol for cultivation of primary PMCs (23), we re-evaluated the culture conditions of the PMC cell lines after noticing cellular transformation. The reason for this was, that we observed an enormous proliferation of both cell lines under primary PMC cultivation conditions, which we thought could have

negative consequences for genomic stability after long-term cultivation of the cells due to the accumulation of additional mutations. Indeed, it has been shown that extremely proliferating tumour cells and inflammation-induced proliferation favour the accumulation of genetic mutations (65, 66) and we could observe by staining pH2Ax that the frequency of DNA double strand breaks was slightly enhanced in PMC-306 cells in relation to primary PMCs despite the reduced SCF/FCS growth conditions. Importantly, before establishing the PMC cell lines as a new MC tool, we reduced SCF and FCS concentrations to levels, which did not negatively affect viability of both cell lines. We could also show that reduced SCF and FCS concentrations in culture medium did not affect the experimental outcome with respect to the analysis of protease expression and granularity of the cells. The only parameter that was influenced by increased SCF concentrations was the cell surface localization of KIT, which reportedly internalizes upon SCF binding (59), while expression of other MC surface markers was not changed. Crucially, cell cycle activity and proliferation were still substantially elevated in PMC-306 cells compared to primary PMCs despite reduced SCF and FCS concentrations in the culture medium.

Spontaneous transformation of cells *in vitro* can either occur due to activating mutations in pro-survival pathways and/or genetic loss of tumour suppressor proteins (55). Transformation of cells is often associated with loss of cell type-specific characteristics. We could exclude an activating mutation in the prominent MC growth factor receptor KIT as we could show that SCF supplementation is still required for PMC-306 cell proliferation and PMC-306 cells are still sensitive to KIT inhibition by Imatinib excluding KIT mutations leading to Imatinib resistance. However, we found complete loss of expression of the two central cell cycle regulators *Cdkn2a* and *Arf* both located on the heterozygously deleted region of chromosome 4. While p16/INK4A inhibits CDK4 and CDK6, thereby preventing entry into S phase by activation of RB (67), p19/ARF inhibits the ubiquitin ligase MDM2, which leads to p53 stabilization and, amongst others, initiation of apoptosis (68, 69). Thus, absence of both of these proteins fuels the cell cycle, circumvents cell cycle control and accelerates cell proliferation as quantified for PMC-306 cells by MKI67 and pH3 staining. The rapid proliferation rate is likely accompanied by a reduced time to build up more complex intracellular structures like MC granules, which is in line with the reduced granular content of PMC-306. Importantly, we detected loss of *Cdkn2a* and *Arf* expression also in the independently transformed PMC-303 line, which we did not characterize as extensively as the PMC-306 cell line in this report. However, PMC-303 cells did not show any abnormalities on chromosome 4 suggesting a different mechanism of gene silencing potentially involving epigenetic mechanisms. Interestingly, the PMC-303 cell line had a trisomy 8, which frequently occurs in murine embryonic stem cells and is associated with increased proliferation, genome instability but does not seem to affect cellular differentiation (70, 71). Nevertheless, similar to PMC-306 cells, the PMC-303 cell line retained its MC-like characteristic effector functions and morphology despite transformation. Crucially, as we observed inactivation of the *Cdkn2a/Arf* locus in

two independent MC lines, it is tempting to speculate that the presence of this tumour suppressor locus might be a central player in preventing MC transformation. Still, our evidence does not allow to draw a direct causal connection between lost *Cdkn2a/Arf* expression and cellular transformation as we cannot for certain declare that this mutation is the first to be acquired during transformation. However, it could potentially also be interesting to investigate the role of *Cdkn2a/Arf* in the context of clonal MC diseases like mastocytosis or MC leukemia. So far, a *CDKN2A* mutation was only described in a case report of a patient suffering from MC leukemia with persistent myelodysplastic syndrome (72) without further characterization. As *Cdkn2a/Arf* inactivation appeared to be a recurrent phenomenon in MCs, we suspected that the culture conditions, notably the presence of SCF, might contribute to the regulation of *Cdkn2a/Arf* mRNA expression. In this regard, it is known that activation of the epidermal growth factor receptor (EGFR) correlates with *Cdkn2a* loss in glioblastoma formation (73). Likewise, tyrosine kinase inhibitor resistance of Philadelphia chromosome-positive leukemia correlates with deletion of the *CDKN2* gene (74), and cooperativity between PTEN loss and loss of *Cdkn2a* and *Arf* in histiocytic sarcoma has been reported (75). This wealth of data suggests that activation of RTKs and downstream PI3K-PKB signaling, which induces cyclin expression and accelerates proliferation (60), is necessary for *Cdkn2a/Arf* inactivation. Indeed, we could show that constitutive KIT activation by SCF downregulated *Cdkn2a* and *Arf* expression in BMMCs. SCF-supplemented BMMCs tried to counterbalance the enormous upregulation of *Ccnd1* by KIT activation through upregulation of *Cdkn2a* up to the first 8 weeks, while prolonged SCF-treatment inactivated the negative regulatory cell cycle regulators. It is reported that mitogenic stimuli, like SCF-mediated KIT activation, upregulate *Cdkn2a/Arf* expression to enable better control of cell cycle progression (76–79), which likely accounts for the increased *Cdkn2a* levels within weeks 4–8. A model could be envisaged in which prolonged cultivation in SCF-containing medium might potentially have favoured the selection of cells with an epigenetically silenced or genetically deleted *Cdkn2a/Arf* locus, which ultimately may have overgrown the cells with intact cell cycle regulation. After the loss of *Cdkn2a/Arf* expression, high cyclin expression obviously became unnecessary because normal cyclin levels were sufficient to fuel the cell cycle in the absence of negative regulatory proteins. This may explain the decrease in *Ccnd1* expression at the same time expression of *Cdkn2a/Arf* was lost in SCF-treated BMMCs. In essence, KIT is an abundant RTK present on all types of differentiated MCs and a potent activator of the PI3K-PKB pathway, thus possessing all requirements to induce the above-described cell cycle regulatory changes, which might have ultimately enabled unrestricted proliferation.

In summary, we herein characterized a new murine FcεRI- and MRGPRB2-positive connective tissue type-like MC line displaying similar characteristics to primary PMCs including several advantages. Importantly, the low number of chromosomal abnormalities reflects the WT MC-like behaviour, which is a great

advantage in comparison to RBL-2H3 cells that have been shown to contain a mean chromosome number of 67 (19). Technically, increased proliferation and reduced protease expression of PMC-306 overcomes the problems of cell number limitations and protein degradation in cell lysates using conventional cell lysis conditions (49) related to experiments with primary PMCs. Ultimately, alternatives to isolation of cells from and experiments with laboratory animals are needed to reduce the number of animals sacrificed for research. Thus, establishing new cell lines supports the 3R guidelines (24) and will help to achieve the future aim of ending the use of animals in research in the USA and the European Union (67). This new MC model will therefore sustain future studies on mechanisms and pharmacologic intervention of MC activation.

## Data availability statement

The NGS data have been deposited in NCBI's Gene Expression Omnibus and are accessible through the GEO Series accession number GSE227065 (<https://www.ncbi.nlm.nih.gov/geo/query/acc.cgi?acc=GSE227065>).

## Ethics statement

The animal study was approved by the Governmental Animal Care and Use Committee at the State Agency for Nature, Environment and Consumer Protection, Recklinghausen (LANUV).

## Author contributions

SC, RS, HS, SM, LG, MK, KH and HK-W performed experiments and analyzed the data. SC and MH conceptualized the study. SC wrote the first draft of the manuscript. SC, RW, CL and MH contributed to review and editing. RW, CL and MH contributed to funding acquisition. All authors contributed to the article and approved the submitted version.

## Funding

This work was supported by grants from the Deutsche Forschungsgemeinschaft (DFG). HU794/12-1 and HU794/14-1 to MH, LI1045/6-1 to CL, WE2554/15-1 to RW and ME3431/2-1 to SM.

## Acknowledgments

We thank Thomas Wilhelm (RWTH Aachen University) for proofreading and fruitful discussions. Moreover, we are grateful to Bernhard Lüscher (RWTH Aachen University) for sharing his expertise in mechanisms of cellular transformation. The content of this manuscript previously appeared online as a preprint at bioRxiv (<https://doi.org/10.1101/2023.01.24.525344>) (68).

## Conflict of interest

The authors declare that the research was conducted in the absence of any commercial or financial relationships that could be construed as a potential conflict of interest.

## Publisher's note

All claims expressed in this article are solely those of the authors and do not necessarily represent those of their affiliated organizations, or those of the publisher, the editors and the reviewers. Any product that may be evaluated in this article, or claim that may be made by its manufacturer, is not guaranteed or endorsed by the publisher.

## Supplementary material

The Supplementary Material for this article can be found online at: <https://www.frontiersin.org/articles/10.3389/fimmu.2023.1154416/full#supplementary-material>

### SUPPLEMENTARY FIGURE 1

MC surface marker expression of PMC-306 before and after immortalization. (A) Representative FACS analysis of PMC-306 cells before transformation after 3 weeks under regular PMC culture conditions. FSC/SSC dot plot shows a typical WT PMC population of 93.6% FcεRI and KIT double-positive cells (n=3).

### SUPPLEMENTARY FIGURE 2

Analysis of primary WT PMC and PMC-306 viability under cytokine deprivation conditions. Representative FACS dot plots showing Annexin V and propidium iodide positivity in primary PMCs and PMC-306 cells under IL-3 (n=3) (A) or SCF (n=3) (B) deprivation for 72 hours. The percentage of single positive, double positive, and double negative cells is provided in the associated gates.

### SUPPLEMENTARY FIGURE 3

Analysis of MRGPRB2 activation shows unconventional degranulation and impact on cellular integrity. (A) ELISA measurement of secreted IL-6 (left) or TNF (right) from PMC-306 cells stimulated with increasing concentrations of C48/80 (n=4). (B) BCA assay to determine the protein concentration in cell lysates of PMC-306 cells stimulated with either Ag [20 ng/ml], C48/80 [10 µg/ml] or Mastoparan [30 µM] for the indicated time points (n=3). (C) Representative flow cytometry dot plots and histograms of primary WT PMCs stimulated with either Ag [20 ng/ml] or C48/80 [10 µg/ml] for indicated time points and stained with anti-LAMP1 to determine granule externalization (n=3). Data are shown as mean +SD. (A) Ordinary one-way ANOVA followed by Dunnett multiple comparisons test. (B) Two-way ANOVA followed by Sidák multiple comparisons test.  $p > 0.05$  ns,  $*p < 0.05$ ,  $**p < 0.01$ ,  $***p < 0.001$ ,  $****p < 0.0001$ . Stars indicate the significance level relative to the respective controls.

### SUPPLEMENTARY FIGURE 4

Different culture conditions do not affect the general PMC-306 phenotype. (A–I) PMC-306 cells were cultivated either under reduced conditions with 10% FCS and 5 ng/ml SCF or primary PMC conditions (full, 15% FCS and 20 ng/ml SCF) to analyze potential effects on different culture conditions on gene expression. Primary WT PMCs cultivated under normal PMC conditions served as reference. mRNA expression of *Cdkn2a* (A), *Arf* (B), *Cma1* (C), *Cpa3* (D), *Gzmb* (E), *Mcpt2* (F), *Mcpt4* (G), *Tpsab1* (H) and *Mrgprb2* (I) were analyzed by qPCR. Expression of the respective genes of interest was quantified by the delta  $C_T$  method using *Hprt* as a housekeeping gene (n=3). (J) Representative FACS dot plots and normalized histograms showing expression of FcεRI, KIT, ST2 and CD13 in PMC-306 cells

cultivated either under reduced (blue) or full medium (red) conditions. The upper two panels show frequency distributions relative to an unstained control (grey) while the lower panel shows frequency distribution comparing reduced and full medium conditions. **(K)** Quantification of the FACS surface marker analysis depicted in **(J)** with MFI's showing staining intensities for the respective surface markers as well as FSC and SSC parameters (n=3). **(A–I)** One-way ANOVA followed by Dunnett multiple comparisons test. **(K)** Unpaired, two-tailed Student's *t*-test with Welch's correction. Data are expressed as mean +SD. *p*>0.05 ns, \**p*<0.05, \*\**p*<0.01, \*\*\**p*<0.001, \*\*\*\**p*<0.0001.

#### SUPPLEMENTARY FIGURE 5

Cytogenetic and gene expression analysis of the independently transformed PMC cell line PMC-303. **(A)** Table of all discovered cytogenetic aberrations of mitotic chromosomes of the PMC-306 cell line with associated frequencies. **(B)** Representative G-banded karyotype of the PMC-303 cell line with trisomy 8 due to a homologous Robertsonian translocation of chromosome 8 (Rb (8.8)). **(D–H)** RT-qPCR analysis of genes encoded within in the region of chromosome 4, which is deleted in the PMC-306 cell line (Chr4 qC4-qC7). Gene expression of *Cdkn2a*, *Arf*, *Rbl1*, *Mllt3*, *Dennd4c* and *Plaa* were measured in PMC-303 cells in comparison to primary WT PMCs (n=3). Data are expressed as mean +SD. Unpaired, two-tailed Student's *t*-test with Welch's correction. \**p*<0.05.

#### SUPPLEMENTARY FIGURE 6

Characterization of the PMC-303 cell line. **(A)** Representative FACS histograms showing surface localization of FcεRI, KIT, ST2 and CD13 in PMC-303 cells after freeze-thaw relative to an unstained control (n=3). **(B)** Representative electron micrographs showing the ultrastructure of PMC-303 cells. **(C)** Quantification of the relative β-hexosaminidase activity in lysates of primary PMCs and PMC-303 cells determined by an enzymatic assay to quantify the amount of cellular β-hexosaminidase expressed in primary PMCs and PMC-306 cells (n=3). **(D)** Determination of the degranulation of PMC-303 cells in response to indicated concentrations of C48/80 assessed by β-hexosaminidase release assay (n=3). **(E)** Determination of the degranulation of PMC-303 cells in response to indicated concentrations of Mastoparan assessed by β-hexosaminidase release assay (n=3). **(F)** FACS analysis of PMC-

303 cells stimulated with Ag [20 ng/ml] for indicated time points to determine externalization of LAMP1 externalization. Bar graphs shown MFI's for LAMP1 for each time point (n=3). **(G)** The pro-inflammatory cytokine production of PMC-303 cells to Ag (20 ng/ml) in comparison to other stimuli (SCF: 100 ng/ml, SCF+Ag: 100 ng/ml and 20 ng/ml, LPS: 1 μg/ml, FSL-1: 1 μg/ml, IL-33: 10 ng/ml, C48/80: 10 μg/ml) was determined by IL-6 ELISA (n=3). **(H)** Same experiment as in **(G)**, but secreted amounts of TNF were determined by ELISA (n=3). Data are expressed as mean +SD. **(C)** Unpaired, two-tailed Student's *t*-test with Welch's correction. **(D–H)** One-way ANOVA followed by Dunnett multiple comparisons test. Stars indicate significance within one group relative to control. *p*>0.05 ns, \**p*<0.05, \*\**p*<0.01, \*\*\**p*<0.001, \*\*\*\**p*<0.0001.

#### SUPPLEMENTARY FIGURE 7

GO Term analysis of the NGS data set, gating strategy and background determination for flow cytometry (FACS) and analysis of aneuploidy. **(A)** For the GO term enrichment analysis all genes regulated at least 5-fold between primary WT PMCs and PMC-306 cells were included. The top 15 GO terms with the lowest *p* values are depicted. GO term analysis was performed using the gene ontology knowledgebase server (<http://geneontology.org/>) **(B–D)** Gating strategy and background determination for the transformed PMC-306 line (red) and primary WT PMCs (black). **(B)** Left panels: Forward versus side scatter (FSC vs. SSC) gating for identification of cells of interest. FSC indicates cell size, SSC indicates cell granularity. Right panels: FSC-A vs. FCS-H gating for identification of single cells. **(C, D)** Unstained controls, which were not incubated with antibodies to assess background for staining against phospho-histone 3 (AL647-A, pH3) and phospho-histone H2Ax (pH2Ax, PerCP-Cy5.5-A) **(C)**, MKI67 (AL700-A) and DAPI (DNA content, BV421-A) **(D)**. **(E)** Representative histograms of primary WT PMCs and PMC-306 cells stained with an antibody directed against MKI67 (AL700-A) and phospho-histone H3 (pH3, AL647-A). Cellular DNA content was determined by DAPI staining (BV421-A) for assignment to the distinct cell cycle phases as follows: SubG1:< 2n DNA content; G1: 2n; S: 2-4n; G2/M: 4n; Aneuploidy: > 4n. Representative overlay of FACS-histograms of DNA content in all single cells (black) versus MKI67+ (yellow, left) or pH3+ (red, right) single cells (normalized to mode). Black arrows indicate MKI67+ and pH3+ cells with a DNA content above 4n (aneuploidy) (n=3).

## References

- Galli SJ, Gaudenzio N, Tsai M. Mast cells in inflammation and disease: Recent progress and ongoing concerns. *Annu Rev Immunol* (2020) 38:49–77. doi: 10.1146/annurev-immunol-071719-094903
- Galli SJ, Tsai M. Mast cells in allergy and infection: versatile effector and regulatory cells in innate and adaptive immunity. *Eur J Immunol* (2010) 40(7):1843–51. doi: 10.1002/eji.201040559
- Metz M, Maurer M. Mast cells—key effector cells in immune responses. *Trends Immunol* (2007) 28(5):234–41. doi: 10.1016/j.it.2007.03.003
- Johnson C, Huynh V, Hargrove L, Kennedy L, Graf-Eaton A, Owens J, et al. Inhibition of mast cell-derived histamine decreases human cholangiocarcinoma growth and differentiation via c-Kit/Stem cell factor-dependent signaling. *Am J Pathol* (2016) 186(1):123–33. doi: 10.1016/j.ajpath.2015.09.016
- Kondo K, Muramatsu M, Okamoto Y, Jin D, Takai S, Tanigawa N, et al. Expression of chymase-positive cells in gastric cancer and its correlation with the angiogenesis. *J Surg Oncol* (2006) 93(1):33–6. doi: 10.1002/jso.20394
- Malaviya R, Ikeda T, Ross E, Abraham SN. Mast cell modulation of neutrophil influx and bacterial clearance at sites of infection through TNF-α. *Nature* (1996) 381(6577):77–80. doi: 10.1038/381077a0
- Zimmermann C, Troeltsch D, Giménez-Rivera VA, Galli SJ, Metz M, Maurer M, et al. Mast cells are critical for controlling the bacterial burden and the healing of infected wounds. *Proc Natl Acad Sci USA* (2019) 116(41):20500–4. doi: 10.1073/pnas.1908816116
- Rathore APS, St John AL. Protective and pathogenic roles for mast cells during viral infections. *Curr Opin Immunol* (2020) 66:74–81. doi: 10.1016/j.coi.2020.05.003
- Ramirez-GarciaLuna JL, Chan D, Samberg R, Abou-Rjeili M, Wong TH, Li A, et al. Defective bone repair in mast cell-deficient Cpa3Cre/+ mice. *PLoS One* (2017) 12(3):e0174396. doi: 10.1371/journal.pone.0174396
- Grimbaldeston MA, Nakae S, Kalesnikoff J, Tsai M, Galli SJ. Mast cell-derived interleukin 10 limits skin pathology in contact dermatitis and chronic irradiation with ultraviolet b. *Nat Immunol* (2007) 8(10):1095–104. doi: 10.1038/ni1503
- Maurer M, Theoharides T, Granstein RD, Bischoff SC, Bienenstock J, Henz B, et al. What is the physiological function of mast cells? *Exp Dermatol* (2003) 12(6):886–910. doi: 10.1111/j.0906-6705.2003.0109a.x
- Huber M, Cato ACB, Ainooson GK, Freichel M, Tsvilovskyy V, Jessberger R, et al. Regulation of the pleiotropic effects of tissue-resident mast cells. *J Allergy Clin Immunol* (2019) 144(4S):S31–45. doi: 10.1016/j.jaci.2019.02.004
- Butterfield JH, Weiler D, Dewald G, Gleich GJ. Establishment of an immature mast cell line from a patient with mast cell leukemia. *Leuk Res* (1988) 12(4):345–55. doi: 10.1016/0145-2126(88)90050-1
- Laidlaw TM, Steinke JW, Tiñana AM, Feng C, Xing W, Lam BK, et al. Characterization of a novel human mast cell line that responds to stem cell factor and expresses functional FcεRI. *J Allergy Clin Immunol* (2011) 127(3):815. doi: 10.1016/j.jaci.2010.12.1101
- Kirshenbaum AS, Akin C, Wu Y, Rottem M, Goff JP, Beaven MA, et al. Characterization of novel stem cell factor responsive human mast cell lines LAD 1 and 2 established from a patient with mast cell sarcoma/leukemia; activation following aggregation of FcεRI or FcγRIIb. *Leuk Res* (2003) 27(8):677–82. doi: 10.1016/S0145-2126(02)00343-0
- Eccleston E, Leonard BJ, Lowe JS, Welford HJ. Basophilic leukaemia in the albino rat and a demonstration of the basopoietin. *Nat New Biol* (1973) 244(133):73–6. doi: 10.1038/newbio244073b0
- Rupp B, Löhning M, Werenskiöld AK. Reversible expression of tryptases in continuous L138.8A mast cells. *Eur J Immunol* (2000) 30(10):2954–61. doi: 10.1002/1521-4141(200010)30:10<2954::AID-IMMU2954>3.0.CO;2-S
- Haenisch B, Herms S, Molderings GJ. The transcriptome of the human mast cell leukemia cells HMC-1.2: an approach to identify specific changes in the gene expression profile in KitD816V systemic mastocytosis. *Immunol Res* (2013) 56(1):155–62. doi: 10.1007/s12026-013-8391-1
- Barsumian EL, Isersky C, Petrino MG, Siraganian RP. IgE-induced histamine release from rat basophilic leukemia cell lines: Isolation of releasing and nonreleasing clones. *Eur J Immunol* (1981) 11(4):317–23. doi: 10.1002/eji.1830110410

20. Passante E, Frankish N. The RBL-2H3 cell line: Its provenance and suitability as a model for the mast cell. *Inflamm Res* (2009) 58(11):737–45. doi: 10.1007/s00011-009-0074-y
21. Xing W, Austen KF, Gurish MF, Jones TG. Protease phenotype of constitutive connective tissue and of induced mucosal mast cells in mice is regulated by the tissue. *Proc Natl Acad Sci USA* (2011) 108(34):14210–5. doi: 10.1073/pnas.1111048108
22. Bischoff SC. Role of mast cells in allergic and non-allergic immune responses: comparison of human and murine data. *Nat Rev Immunol* (2007) 7(2):93–104. doi: 10.1038/nri2018
23. Meurer SK, Neß M, Weiskirchen S, Kim P, Tag CG, Kauffmann M, et al. Isolation of mature (Peritoneum-derived) mast cells and immature (Bone marrow-derived) mast cell precursors from mice. *PLoS One* (2016) 11(6):e0158104–e0158104. doi: 10.1371/journal.pone.0158104
24. Justin M, Jež M, Košir A, Miceska S, Rožman P, Jazbec K. Application of the 3R principles: Vertebrae as an additional source of murine bone-marrow cells. *Lab Anim* (2021) 55(1):43–52. doi: 10.1177/0023677220922573
25. Kamijo T, Zindy F, Roussel MF, Quelle DE, Downing JR, Ashmun RA, et al. Tumor suppression at the mouse INK4a locus mediated by the alternative reading frame product p19ARF. *Cell* (1997) 91(5):649–59. doi: 10.1016/S0092-8674(00)80452-3
26. Sharpless NE. INK4a/ARF: a multifunctional tumor suppressor locus. *Mutat Res* (2005) 576(1–2):22–38. doi: 10.1016/j.mrfmmm.2004.08.021
27. Karasuyama H, Melchers F. Establishment of mouse cell lines which constitutively secrete large quantities of interleukin 2, 3, 4 or 5, using modified cDNA expression vectors. *Eur J Immunol* (1988) 18(1):97–104. doi: 10.1002/eji.1830180115
28. Nishizumi H, Yamamoto T. Impaired tyrosine phosphorylation and Ca<sup>2+</sup> mobilization, but not degranulation, in Lyn-deficient bone marrow-derived mast cells. *J Immunol* (1997) 158(5):2350–5. doi: 10.4049/jimmunol.158.5.2350
29. Pfaffl MW. A new mathematical model for relative quantification in real-time RT-PCR. *Nucleic Acids Res* (2001) 29(9):e45–5. doi: 10.1093/nar/29.9.e45
30. Liu L, Damen JE, Cutler RL, Krystal G. Multiple cytokines stimulate the binding of a common 145-kilodalton protein to shc at the Grb2 recognition site of shc. *Mol Cell Biol* (1994) 14(10):6926–35. doi: 10.1128/mcb.14.10.6926-6935.1994
31. Shaffer LG, Tommerup N. *ISCN 2005: an international system for human cytogenetic nomenclature (2005): recommendations of the international standing committee on human cytogenetic nomenclature*. Karger Medical and Scientific Publishers (2005). Available at: <https://www.ncbi.nlm.nih.gov/nlmcatalog?cmd=PureSearch&term=101256672%5Bnlmid%5D>.
32. Islam MQ, Levan G. A new fixation procedure for improved quality G-bands in routine cytogenetic work. *Hereditas* (1987) 107(1):127–30. doi: 10.1111/j.1601-5223.1987.tb00277.x
33. Korf BR, Schuh BE, Salwen MJ, Warburton D, Miller OJ. The role of trypsin in the pre-treatment of chromosomes for giemsa banding. *Hum Genet* (1976) 31(1):27–33. doi: 10.1007/BF00270396
34. Ewels PA, Peltzer A, Fillinger S, Patel H, Alneberg J, Wilm A, et al. The nf-core framework for community-curated bioinformatics pipelines. *Nat Biotechnol* (2020) 38:276–8. United States. doi: 10.1038/s41587-020-0439-x
35. Di Tommaso P, Chatzou M, Floden EW, Barja PP, Palumbo E, Notredame C. Nextflow enables reproducible computational workflows. *Nat Biotechnol* (2017) 35:316–9. United States. doi: 10.1038/nbt.3820
36. Merkel D. Docker: Lightweight Linux containers for consistent development and deployment. *Linux J* (2014) 2014:2.
37. Krueger F, James F, Ewels P, Afyounian E, Schuster-Boeckler B. (2021) *FelixKrueger/TrimGalore: v0.6.7 - DOI via Zenodo (0.6.7)*. Zenodo. doi: 10.5281/zenodo.5127899
38. Dobin A, Davis CA, Schlesinger F, Drenkow J, Zaleski C, Jha S, et al. STAR: ultrafast universal RNA-seq aligner. *Bioinformatics* (2013) 29(1):15–21. doi: 10.1093/bioinformatics/bts635
39. Patro R, Duggal G, Love MI, Irizarry RA, Kingsford C. Salmon provides fast and bias-aware quantification of transcript expression. *Nat Methods* (2017) 14(4):417–9. doi: 10.1038/nmeth.4197
40. Wernersson S, Pejler G. Mast cell secretory granules: Armed for battle. *Nat Rev Immunol* (2014) 14(7):478–94. doi: 10.1038/nri3690
41. Furitsu T, Tsujimura T, Tono T, Ikeda H, Kitayama H, Koshimizu U, et al. Identification of mutations in the coding sequence of the proto-oncogene c-kit in a human mast cell leukemia cell line causing ligand-independent activation of c-kit product. *J Clin Invest* (1993) 92(4):1736–44. doi: 10.1172/JCI116761
42. Nilsson G, Blom T, Kusche-Gullberg M, Kjellén L, Butterfield JH, Sundström C, et al. Phenotypic characterization of the human mast-cell line HMC-1. *Scand J Immunol* (1994) 39(5):489–98. doi: 10.1111/j.1365-3083.1994.tb03404.x
43. Valent P, Akin C, Hartmann K, Nilsson G, Reiter A, Hermine O, et al. Advances in the classification and treatment of mastocytosis: Current status and outlook toward the future. *Cancer Res* (2017) 77(6):1261–70. doi: 10.1158/0008-5472.CAN-16-2234
44. Metcalfe DD. Mast cells and mastocytosis. *Blood* (2008) 112(4):946–56. doi: 10.1182/blood-2007-11-078097
45. Huber M. Activation/Inhibition of mast cells by supra-optimal antigen concentrations. *Cell Commun Signal* (2013) 11(1):7. doi: 10.1186/1478-811X-11-7
46. McNeil BD, Pundir P, Meeke S, Han L, Udem BJ, Kulka M, et al. Identification of a mast-cell-specific receptor crucial for pseudo-allergic drug reactions. *Nature* (2015) 519(7542):237–41. doi: 10.1038/nature14022
47. Plum T, Wang X, Rettel M, Krijgsveld J, Feyerabend TB, Rodewald H-R. Human mast cell proteome reveals unique lineage, putative functions, and structural basis for cell ablation. *Immunity* (2020) 52(2):404–416.e5. doi: 10.1016/j.immuni.2020.01.012
48. Pundir P, Liu R, Vasavda C, Serhan N, Limjunyawong N, Yee R, et al. A connective tissue mast-Cell-Specific receptor detects bacterial quorum-sensing molecules and mediates antibacterial immunity. *Cell Host Microbe* (2019) 26(1):114–122.e8. doi: 10.1016/j.chom.2019.06.003
49. Malbec O, Roget K, Schiffer C, Iannascoli B, Dumas AR, Arock M, et al. Peritoneal cell-derived mast cells: an *in vitro* model of mature serosal-type mouse mast cells. *J Immunol* (2007) 178(10):6465–75. doi: 10.4049/jimmunol.178.10.6465
50. Drube S, Heink S, Walter S, Löhn T, Grusser M, Gerbaulet A, et al. The receptor tyrosine kinase c-kit controls IL-33 receptor signaling in mast cells. *Blood* (2010) 115(19):3899–906. doi: 10.1182/blood-2009-10-247411
51. Eklund KK, Ghildyal N, Austen KF, Friend DS, Schiller V, Stevens RL. Mouse bone marrow-derived mast cells (mBMMC) obtained *in vitro* from mice that are mast cell-deficient *in vivo* express the same panel of granule proteases as mBMMC and serosal mast cells from their normal littermates. *J Exp Med* (1994) 180(1):67–73. doi: 10.1084/jem.180.1.67
52. Lunderius C, Xiang Z, Nilsson G, Hellman L. Murine mast cell lines as indicators of early events in mast cell and basophil development. *Eur J Immunol* (2000) 30(12):3396–402. doi: 10.1002/1521-4141(200012)30:12<3396::AID-IMMU3396>3.0.CO;2-O
53. Wu Y, Renard C-A, Apiou F, Huerre M, Tiollais P, Dutrillaux B, et al. Recurrent allelic deletions at mouse chromosomes 4 and 14 in myc-induced liver tumors. *Oncogene* (2002) 21(10):1518–26. doi: 10.1038/sj.onc.1205208
54. Sherr CJ. The INK4a/ARF network in tumour suppression. *Nat Rev Mol Cell Biol* (2001) 2(10):731–7. doi: 10.1038/35096061
55. Hanahan D, Weinberg RA, Francisco S. The hallmarks of cancer. *Cell* (2000) 100:57–70. doi: 10.1016/S0092-8674(00)81683-9
56. Matthews HK, Bertoli C, de Bruin RAM. Cell cycle control in cancer. *Nat Rev Mol Cell Biol* (2022) 23(1):74–88. doi: 10.1038/s41580-021-00404-3
57. Sherr CJ, McCormick F. The RB and p53 pathways in cancer. *Cancer Cell* (2002) 2(2):103–12. doi: 10.1016/S1535-6108(02)00102-2
58. Sundström M, Vliagoftis H, Karlberg P, Butterfield JH, Nilsson K, Metcalfe DD, et al. Functional and phenotypic studies of two variants of a human mast cell line with a distinct set of mutations in the c-kit proto-oncogene. *Immunology* (2003) 108(1):89–97. doi: 10.1046/j.1365-2567.2003.01559.x
59. Shimizu Y, Ashman LK, Du Z, Schwartz LB. Internalization of kit together with stem cell factor on human fetal liver-derived mast cells: New protein and RNA synthesis are required for reappearance of kit. *J Immunol* (1996) 156(9):3443–9. doi: 10.4049/jimmunol.156.9.3443
60. Reyes-Sebastian J, Montiel-Cervantes LA, Reyes-Maldonado E, Dominguez-Lopez ML, Ortiz-Butron R, Castillo-Alvarez A, et al. Cell proliferation and inhibition of apoptosis are related to c-kit activation in leukaemic lymphoblasts. *Hematology* (2018) 23(8):486–95. doi: 10.1080/10245332.2018.1444564
61. Green DP, Limjunyawong N, Gour N, Pundir P, Dong X. A mast-Cell-Specific receptor mediates neurogenic inflammation and pain. *Neuron* (2019) 101(3):412–420.e3. doi: 10.1016/j.neuron.2019.01.012
62. Gaudenzio N, Sibilano R, Marichal T, Starkl P, Reber LL, Cenac N, et al. Different activation signals induce distinct mast cell degranulation strategies. *J Clin Invest* (2016) 126(10):3981–98. doi: 10.1172/JCI85538
63. Haase D, Feuring-Buske M, Könemann S, Fonatsch C, Troff C, Verbeek W, et al. Evidence for malignant transformation in acute myeloid leukemia at the level of early hematopoietic stem cells by cytogenetic analysis of CD34+ subpopulations. *Blood* (1995) 86(8):2906–12. doi: 10.1182/blood.V86.8.2906.2906
64. Ball PE, Conroy MC, Heusser CH, Davis JM, Conscience JF. Spontaneous, *in vitro*, malignant transformation of a basophil/mast cell line. *Differentiation* (1983) 24(1):74–8. doi: 10.1111/j.1432-0436.1983.tb01305.x
65. Kiraly O, Gong G, Olipitz W, Muthupalani S, Engelward BP. Inflammation-induced cell proliferation potentiates DNA damage-induced mutations *in vivo*. *PLoS Genet* (2015) 11(2):e1004901. doi: 10.1371/journal.pgen.1004901
66. Grzywa TM, Koppolu AA, Paskal W, Klicka K, Rydzanicz M, Wejman J, et al. Higher mutation burden in high proliferation compartments of heterogeneous melanoma tumors. *Int J Mol Sci* (2021) 22(8):3886. doi: 10.3390/ijms22083886
67. Serrano M, Hannon GJ, Beach D. A new regulatory motif in cell-cycle control causing specific inhibition of cyclin D/CDK4. *Nature* (1993) 366(6456):704–7. doi: 10.1038/366704a0
68. Weber JD, Taylor LJ, Roussel MF, Sherr CJ, Bar-Sagi D. Nucleolar arf sequesters Mdm2 and activates p53. *Nat Cell Biol* (1999) 1(1):20–6. doi: 10.1038/8991
69. Honda R, Yasuda H. Association of p19(ARF) with Mdm2 inhibits ubiquitin ligase activity of Mdm2 for tumor suppressor p53. *EMBO J* (1999) 18(1):22–7. doi: 10.1093/emboj/18.1.22
70. Gaztelumendi N, Nogués C. Chromosome instability in mouse embryonic stem cells. *Sci Rep* (2014) 4(1):5324. doi: 10.1038/srep05324
71. Kim YM, Lee J-Y, Xia L, Mulvihill JJ, Li S. Trisomy 8: A common finding in mouse embryonic stem (ES) cell lines. *Mol Cytogenet* (2013) 6(1):3. doi: 10.1186/1755-8166-6-3
72. Yang J, Gabali A. Mast cell leukemia and hemophagocytosis in a patient with myelodysplastic syndrome. *Blood* (2019) 133(20):2243. doi: 10.1182/blood.201886564

73. Acquaviva J, Jun HJ, Lessard J, Ruiz R, Zhu H, Donovan M, et al. Chronic activation of wild-type epidermal growth factor receptor and loss of Cdkn2a cause mouse glioblastoma formation. *Cancer Res* (2011) 71(23):7198–206. doi: 10.1158/0008-5472.CAN-11-1514
74. Xu N, Li Y, Li X, Zhou X, Cao R, Li H, et al. Correlation between deletion of the CDKN2 gene and tyrosine kinase inhibitor resistance in adult Philadelphia chromosome-positive acute lymphoblastic leukemia. *J Hematol Oncol* (2016) 9:40. doi: 10.1186/s13045-016-0270-5
75. Carrasco DR, Fenton T, Sukhdeo K, Protopopova M, Enos M, You MJ, et al. The PTEN and INK4A/ARF tumor suppressors maintain myelolymphoid homeostasis and cooperate to constrain histiocytic sarcoma development in humans. *Cancer Cell* (2006) 9(5):379–90. doi: 10.1016/j.ccr.2006.03.028
76. de Stanchina E, McCurrach ME, Zindy F, Shieh SY, Ferbeyre G, Samuelson AV, et al. E1A signaling to p53 involves the p19(ARF) tumor suppressor. *Genes Dev* (1998) 12(15):2434–42. doi: 10.1101/gad.12.15.2434
77. Zindy F, Eischen CM, Randle DH, Kamijo T, Cleveland JL, Sherr CJ, et al. Myc signaling via the ARF tumor suppressor regulates p53-dependent apoptosis and immortalization. *Genes Dev* (1998) 12(15):2424–33. doi: 10.1101/gad.12.15.2424
78. Palmero I, Pantoja C, Serrano M. p19ARF links the tumour suppressor p53 to ras. *Nature* (1998) 395:125–6. doi: 10.1038/25870
79. DeGregori J, Leone G, Miron A, Jakoi L, Nevins JR. Distinct roles for E2F proteins in cell growth control and apoptosis. *Proc Natl Acad Sci USA* (1997) 94(14):7245–50. doi: 10.1073/pnas.94.14.7245